AN ATTEMPT TO CORRELATE BIMODAL FATIGUE ENDURACE DISTRIBUTIONS IN OFHC COPPER WITH WOOD's H, F AND S RANGES

by

D. B. Muggeridge

Manuscript received October 21, 1966

JUNE 1967 UTIAS TECHNICAL NOTE 111

ACKNOWLEDGEMENTS

The author is indebted to Dr. G.N. Patterson, Director of the University of Toronto Institute for Aerospace Studies, for providing the opportunity to work on this project, and to Dr. G. K. Korbacher for his interest in the progress of the work and the supervision of the project.

The author also wishes to thank Dr. W. A. Wood, Professor in the Institute for the Study of Fatigue and Reliability, Columbia University for his guidance and review of the final manuscript.

The help given to the author by Mr. W. Hoppe, Metallurgist, De Havilland Aircraft of Canada, Limited, is also gratefully acknowledged.

This research program was sponsored jointly by the National Aeronautics and Space Administration and the National Research Council of Canada.

SUMMARY

This note presents the results of a metallographic study of a sampling of annealed and then fine machined OFHC copper specimens from statistically meaningful samples, fatigued under constant amplitude tension-compression. An attempt was made to correlate their microstructure with that characteristic of W. A. Wood's H, and F amplitude ranges of the generalized S-N curve.

The sampling specimens for the microstructural examination were taken from the tail ends of the endurance distributions at each of four stress levels around the lower knee of the S-N curve. The microstructural evidence and data from appropriate mechanical tests show that the fatigue mechanisms responsible for failure are H and F. Transition from H to F with decreasing stress level demonstrates the co-existence of the H and F fatigue mechanisms and suggests a bimodal distribution of endurances.

For comparative purposes, a small group of re-annealed electro-polished specimens was also examined. Observations on crack tip profiles support Laird's recently published work on the plastic relaxation process in crack propagation.

TABLE OF CONTENTS

I. INTRODUCTION

Over the years a large amount of fatigue data, traditionally presented as stress (S)-endurance (N) curves, has been reported for a variety of metals. These S-N curves follow much the same slope for different metals. Manson and Coffin (Refs. 1 and 2) have in fact pointed out that it is possible to describe large ranges of the curves by the same power function, using appropriate parameters. However, these formulae neither describe the fatigue mechanisms nor define or identify the microstructural changes responsible for these ranges.

Distinct microstructural differences, which W. A. Wood (Ref. 3) observed in his search for the underlying fatigue mechanisms led him to divide the generalized S-N curve into three ranges (H, F and S). It should be noted, however, that between these ranges there are transition regions where one range predominates in co-existence with the others. Further, Wood has correlated amplitudes in cyclic stress-strain tests with amplitudes in the S-N test .

At about the same time, the already recognized fact that the failure life distribution of materials is a statistical phenomenon was taken into consideration in actual fatigue testing. The endurances of constant amplitude tests were found to closely follow log-normal or extremal distribution functions. The endurance scatter band (variance) was observed to increase as the stress amplitudes decrease. Such behaviour could suggest a kind of transition from one fatigue mechanism to another. Discontinuities in the S-N curve of aluminum (Refs. 4, 5, 6, 7 and 8) of polycrystalline copper (Ref. 9) single copper crystals (Ref. 10) and steel (Refs. 12 and 13) have also been reported.

Discontinuities in polycrystalline metals have been interpreted and presented as a blending of two endurance distributions (e.g. Refs. 8 and 13). Such a blending is postulated as being caused by the decay in probability of occurrence of one failure mechanism and the growth of another. At any stress amplitude within the transition region, there is a finite probability that either mechanism may cause failure.

Frost in Ref. 14 has discussed the phenomenon of the discontinuity in the S-N curves from a metallurgical standpoint. He suggests that the mechanism of fatigue damage changes from (intercrystalline) cracking at subgrain boundaries above the knee to (transcrystalline) slip band cracking below it.

Nine in Ref. 10 has concluded from work on <111> Copper single crystals, that a discontinuity exists at the lower knee of the S-N curve and one at a higher amplitude. He further suggests that the lower branch corresponds to the low-amplitude (F) range, and that the two upper branches correspond to the high-amplitude (H) range. In Ref. 11, a study of fatigue of copper single crystals of [100] axial orientation indicated the existance of a threshold strain, which divides the S-N curve into the H and F ranges without any transition region.

II. FATIGUE MACHINE, MATERIAL AND TEST PROCEDURE

For a more detailed description than that give below, see Ref. 15.

2.1 The Fatigue Machine

The machine used for fatiguing the specimens was a resonance type, tension-compression fatigue machine (see Figs. 1 and 2). A 25 lb. maximum load, electromagnetic shaker provided the driving force. The force was transmitted to the specimen via a lever connected at one end to the shaker and at the other end to the oscillating lower gripping head (the upper one was stationary) via two vertical flat steel plates. Strain gauges on these plates served as a dynamometer. A coil spring, attached to the lever and to the frame, provided a means of applying a mean stress (which was kept zero in this test series). The input was supplied by an amplified sine wave audio oscillator. The resonant frequency of the system was about 80 cps.

2.2 The Fatigue Specimen and Its Material

The specimen profile is shown in Fig. 3. This particular configuration was adopted after consulting photo-elastic specimen models to keep stress concentrations as low as possible.

The specimen material was Certified OFHC copper-121 supplied by Anaconda Company (Canada). OFHC copper conforms to ASTM Specification B-170-47. The Certified OFHC brand copper meets the following requirements in addition to ASTM conformance:

Copper	99.96 per cent by weight min.
Phosphorous	less than 0.003 per cent
Sulphur	less than 0.0040 per cent
Zinc	less than 0.0003 per cent
Mercury	less than 0.0001 per cent
Lead	less than 0.0010 per cent

Although the copper content of Certified OFHC copper is given as 99.96 min., the Anaconda Company reports that some investigators have found copper contents of 99.997% in this material.

The material was delivered in batches of 3/4" diameter, 12' rods in the 1/2 hard cold drawn condition. The specimens were rough machined to 0.025 in. oversize in the test length. Then they were annealed hanging (to prevent eccentricity) for 2 hours at 1050°F in a vacuum of 25 microns of Hg. in bathces of 200. The final machining consisted of 5 fine lathe cuts of 0.0025 in. depth and 0.002 in. feed per revolution.

To determine the mechanical properties of the material six or seven control specimens were taken at random from each of the four heat treatment batches. The mechanical properties of these 27 specimens are listed in Table I. The hardness values were obtained by placing the impressions on the ends of the specimens where no machining had been done subsequent to annealing.

2.3 Test Procedure

The testing was performed with the utmost care to keep experimental errors to a minimum. Relevant specimen dimensions were measured prior to insertion in the machine.

For testing, specimens fatigued at a particular stress amplitude were taken from one heat treatment batch only. Thus, 133 specimens from batach A were tested at $\pm$ 14.0 ksi; 148 specimens from batch B were tested at $\pm$ 13.0 ksi; 200 specimens from batch C were tested at $\pm$ 16.5 ksi; 148 specimens from batch D were tested at $\pm$ 12.7 ksi.

During each test a record was kept of any temperature and humidity fluctuations.

III. MECHANICAL TESTING AND METALLOGRAPHIC EXAMINATION

3.1 Examination of Unfatigued Specimens

The tensile specimens' fracture surfaces were investigated and one typical surface is shown in Fig. 4. A view of one half of the fracture surface (Fig. 5) shows the three regions that failed by different mechanisms as reported by Rogers in Ref. 16. Stage I is the formation, growth and coalescence of individual voids in the central region of the neck to form the central crack. Due to the fine grain size it is believed that there is only a small region of large void coalescence before Stage II begins. In Stage II the crack produced in Stage I propogates by causing a shear strain localization at its tip and at a large angle to the transverse plane. An array of small voids is nucleated in the thin sheet of heavily deformed material in the central region of the neck. This void-weakened region fails under the action of the applied tensile stress. Finally in Stage III the tensile failure is by a mechanism that results in the "double-cup" fracture shown in Fig. 5. It has been suggested by Rogers in Ref. 16 that this Stage III mechanism is the same as the mechanism of nongrain-boundary void growth.

All our "double-cup" fracture surfaces exhibited some bright facets of brittle fracture at the center and a region of shear failure right at the lip of the fracture surface. This shear failure may have been caused by the work-hardened surface layer.

Longitudinal and transverse sections (see Fig. 6a) from unfatigued specimens were prepared to establish the hardness of the material together with the grain size and its uniformity across the section. These sections were obtained by standard mechanical polishing methods and finished by a 30 second electropolish in an orthophosphoric acid solution.

Macrohardness surveys indicated a Vickers Diamond Pyramid Hardness Number of 46.2 for the longitudinal sections and 50.7 for the transverse sections. These values represent the mean values of four impressions made on 16 longitudinal and 16 transverse sections. The difference between the longitudinal and transverse hardness values indicated an annealing texture.

The grain size, typical of all heat treatment batches, was that of ASTM No. 8 (0.027 mm. average grain diameter). Recrystallization was only

partially complete and the grain structure was approximately 50 per cent polygonized (see Fig. 7).

The grain structure was uniform in the core region of the specimen, but a work hardened surface layer was found on all specimens. This feature was due to the fact that 0.025 inches was removed, by fine machining, from the diameter of the specimens after they had been annealed. The work hardened surface layer was approximately ten-thousanths of an inch thick. This depth was established by reducing the diameter of the specimen by electropolishing in orthophosphoric acid until the core gave x-ray back reflection patterns typical of annealed material. Figure 8 shows such a pattern for the fine grained annealed structure of the core of all specimens. The depth of the work hardened layer of ten thousanths of an inch was also confirmed by direct measurements of sections.

To establish the state of the surface as a result of final machining, specimens were silverplated before sectioning. This ensured good preservation of surface contours. The upper section shown in Fig. 6b was used to obtain a taper magnification in addition to the optical magnification. The taper magnification was obtained by polishing a shallow flat on the surface. It is defined as csc α where α is the angle which defines the width of the flat. It is obvious from Figs. 9, 10, 11, and 12 that a "rough" surface had been left by the lathe tool. This surface was the result of the sharpness of the tool (Figs. 9 and 10), its shape (Fig. 11), and emery paper (Fig. 12). The photomicrographs referred to are typical of the entire heat treatment batches. Although the surface contours appear radically different, the depth of the work hardened layer was essentially the same for all specimens.

3.2 Examination of fatigued Specimens

All specimens were silverpated and sectioned longitudinally to the diameter. This ensured good surface preservation and enabled observations to be made on the core at a standard sectioning depth. This case is shown in the lower section of Fig. 6b.

Specimens were taken from each of four stress amplitudes in the vicinity of the lower knee. Particular attention was given to specimens, the endurances of which at a specific stress level fell at the extreme ends (see Fig. 13) of the fatigue life range. Figures 14, 15, 16 and 17 show the endurance histograms for all specimens tested. The specimen numbers shown in these figures refer to specimens singled out for examination. These numbers are used to reference all photomicrographs of such specimens. All sections were prepared by mechanical polishing followed by electropolishing in orthophosphoric acid solution. A standard Ferric-chloride reagent was used.

3.2.1 The Specimen Surface

No surface disturbances were observed other than microcracks that originated at the root of the grooves left by the lathe tool during final maching. (See Fig. 18). It should be noted that there are several separate microcracks linking up in the cold-worked surface layer. This layer etches up much as an H region, produced by especially high amplitudes, would.

Some microcracking occurred at the interface between the cold-worked layer and the annealed core and caused the surface layer to spall. Cold-work enforces dispersal of slip, that would otherwise concentrate in slip zones. It does it by multiplying dislocations and dislocation sources, thus promoting the spread of subsequent slip. Furthermore, cold-work disorients the grains, thus shortening the length of individual slip paths. As a result, no slip zones were observed on or near the surface of any specimen.

3.2.2 Wood's H, F, and S Ranges

The annealed core of the specimens demonstrated the H, F and S range fatigue damage as reported by Wood (Ref. 3). His three ranges divide the generalized S-N curve for this material (fcc) as shown in Fig. 19. The H range is the large-amplitude range, where endurance slowly increases with decreasing amplitude; F is the small-amplitude range where endurance rapidly increases; and, S the still smaller-amplitude range where life becomes infinitely long. At H amplitudes, grains progressively disorient, deform inhomogeneously and strain-harden. At F and S amplitudes, grains do none of these things.

Each range, according to Wood, has its distinctive microstructural characteristics. Distorted slip-zones are common features of the F and S ranges. In the S range slip movements disperse and grains deform as uniformly as they can. In the F range, comparable dispersion does not occur. Individual slip zones continue to intensify and then exhibit various signs of damage. Microcrack formation in a distorted slip zone begins with small pores at separate points. With continued cycling the pores multiply and coalesce and finally the whole slip zone becomes one microcrack. Slip zone microcracks, in general, do not seem to be self-propogating. As the final stage of failure is approached the fatigued slip-zones in some part of a grain may become numerous enough to weaken the structure and cause it to collapse locally into a macrocrack. In the H range, cell formation is the characteristic feature. The cells are usually about 1/10 to 1/100 of the original grain size. Macrocracks are initiated by pores, located in the cell boundaries, which multiply during continued cycling and finally coalesce into cavities and microcracks.

It should be noted that talking about the characteristic microstructural features of any of Wood's three ranges does not mean that they exclusively prevail. In practical metals, it only means that in an H range, H predominates, but the characteristic features of the other ranges can also be observed. This is true in particular for the specimens used in this study where the work-hardened surface layer is subjected to a higher stress than that of the core. As a result, a pronounced stress amplitude transition region was observed in which H and F microstructure coexisted.

A visual estimation of the per cent of each of these ranges in a specimen was attempted. This was done by counting the number of grains showing H, F or S fatigue damage. This method was sensitive enough to delineate different percentages of the three ranges at the 4 stress amplitude levels tested, but not sensitive enough to distinguish between the short term life (STF) and the long term life (LTF) specimens fatigued at one and the same stress amplitude. The percentage estimates are as shown in the subsequent table, where they are also compared with the STF and LTF percentages as suggested by the test results of Ref. 15.

Stress amplitude	Microstructure Test Results (Ref. 15)			
(ksi)	Percentage of			
	H	F and S	STF	LTF
± 12.7	5	95	≃ 5	95
± 13.0	30	70	37	63
± 14.0	30	70	33	67
± 16.5	40	60	22	78

The percentages of the H and F range microstructure at a given stress amplitude reasonably agree with the percentages of the apparent STF and LTF fractions (see Ref. 15) of the statistical bimodal endurance distributions.

3.2.3 X-Ray Tests

X-ray reflection patterns are known to provide a convenient method for identifying specimens that had been subjected to H range amplitudes. In such cases the sharp Laue spots obtained from undeformed grains spread out into arcs. Back-reflection patterns obtained from specimens subjected to stress amplitudes of ± 12.7, ± 13.0, ± 14.0 and ± 16.5 ksi are shown in Figs. 20, 21, 22, and 23 respectively. For sake of comparison, Fig. 8, showing the original annealed pattern, should be referred to. The patterns taken along the axis of the sectioned (to the diameter) specimens reveal a gradual disorientation as the stress amplitude increases.

3.2.4 Optical Microscopy

Typical photomicrographs are given of specimens taken from both ends of the four endurance distributions, as indicated in Fig. 13. Figures 24 and 25 show typical features of specimens fatigued at a stress amplitude of ± 12.7 ksi. Both distorted slip zones and coarse cross slip are seen in Fig. 24, whereas Fig. 25 shows distorted slip-zones. A few very small areas of H range damage are to be seen too. Similar distorted slip-zones for a specimen fatigued at a stress amplitude of ± 13.0 ksi are shown in Fig. 26. At a stress amplitude of ±14.0 ksi, more H range damage is in evidence. Figures 27 and 28 show such damage together with fatigued-slip zone damage. Distortion of twin boundaries and cross slip is shown in Fig. 28. Grain boundary damage is evident in both figures. Figures 29, 30 and 21 demonstrate features of specimens fatigued at a stress amplitude of ± 16.5 ksi. Figure 29 shows concentrated fatigued slip-zones together with H range damage. A large area of fine cross slip is shown in Fig. 30, as is the crystallite formation reported by Forsyth in Ref. 17. Figure 31 shows damage at cell boundaries and large deformation of twin boundaries. Etch pitts reveal the difference in orientation within a grain.

Grain boundary and twin boundary damage is to be expected at a wide range of stress amplitudes. Due to the fine grain size of the material

used in the investigation grain boundary damage was greatly emphasized. A typical picture of such damage found in a specimen fatigued at a stress amplitude of ± 14.0 ksi is shown in Fig. 32. The same features are shown in another view of the same specimen (see Fig. 33) together with fatigued slip-zones and fatigued cross slip zone.

3.2.5 Macrohardness Test Values

Macrohardness surveys were taken of the fatigued specimens previously examined. A Vickers Hardness Tester with a Diamond Pyramid Indentor under a 2.5 kg. load was used. All impressions were made on the center line of longitudinal sections reduced to the diameter of the test section. The values shown by solid symbols in Fig. 34 are the means of 4 impressions taken on each of four different specimens. Hardness values for short and long life specimens at stress amplitudes of ± 12.7, ± 13, ± 14, and ± 16.5 ksi are shown. These hardness values were all equal within the limits of accuracy of the hardness tester.

Some specimens were tested at other than the above stress amplitudes to establish fracture hardness values over a wider stress amplitude range. Their hardness values are represented by open symbols in Fig. 34. It should be noted that they represent the mean of four impressions made on only one specimen at each of the indicated stress amplitude.

3.2.6 Microhardness Test Values

Microhardness surveys were made with a Leitz Microhardness Tester using 15 and 100 gram loads. Figure 35 shows an attempt to measure these microhardnesses at specific characteristic spots.

Hardness values were obtained for typical H and F grains in specimens tested at stress amplitudes of ± 12.7, ± 13, ± 14 and ± 16.5 ksi. These hardness values are the means of four impressions made on four specimens taken from each stress level. The actual values are given below:

Stress amplitude (ksi)	Microhardness (D.P.N.) H grain	F grain
± 12.7	78.0	53.5
± 13.0	80.0	61.2
± 14.0	80.9	53.5
± 16.5	81.3	55.9

3.3 Examination of Re-Annealed Specimens

A series of specimens were re-annealed to a grain size given by ASTM No. 4 (0.0898 mm average grain diameter) and electropolished in orthophosphoric acid for 20 minutes before fatiguing. Figure 36 shows a transverse section typical of the unfatigued specimens.

The electropolished surface of the fatigued specimens lent itself to a direct surface study (classical procedure) in addition to studying the surface features and internal change by means of the taper sectioning technique. The sectioning procedure is shown in Fig. 6c.

Figure 37 shows the electropolished surface of a specimen fatigued at a stress amplitude of ± 12.0 ksi. The main crack is perpendicular to the stress axis as reported by Laird (Ref. 20) for Stage II Fatigue. Concentrated slip and deformation bands in the crack vicinity are clearly shown, as are regions of extreme lattice distortion and cross slip. Several areas of the crystallite formation (rumpling of the surface) are seen, that Forsyth reports in Ref. 17 for specimens fatigued at higher stress amplitudes. Figure 38 is a view of a different portion of the same crack at higher magnification. In the center of the photomicrograph, large rumpling of the surface can be noted in the area that protrudes from it. A small region of kink bands are also in evidence at the left center of the surface. Kink bands have been reported by Forsyth (Ref. 17) as a typical of grains fatigued at stress amplitudes above the knee of the S-N curve of sopper.

Taper sectioning of the same specimens (Fig. 39) reveals "slip-zone microcracks". They originate from small pores in distorted slip zones. The pores multiply and coalesce with continued cycling. The final stage of failure occurs when such slip-zone microcracks become numerous enough to locally link up into a macrocrack.

Further observations on the above specimens show typical notch-peak effects as demonstrated in Fig. 40. The notch-peak effect refers to changes in contour where slip movements concentrate for many cycles in one narrow zone which ends at the surface. As shown by Wood (Ref. 3) these contour changes are a consequence of how the to-and-fro slip movements of cyclic strain destribute themselves across the zone on which they are concentrating. Such an explanation seems to be more in keeping with observations than the hypotheses of Mott (Ref. 19) and Cottrell (Ref. 16). Also, Laird in Ref. 20 in his definition of the plastic relaxation process opposes the hypotheses of Mott and Cottrell.

Grain boundaries are always sites of abnormal deformation and therefore potential sites of fatigue damage. When they predominate over competing sites such as slip zones, microcracks follow them. Grain boundary damage is possible under a wide range of stress amplitudes and is observed in the H range as well as in the F and S ranges. A view of a typical grain boundary microcrack is shown in Fig. 41.

3.4 Some Crack Tip Profile Observations

Several specimens revealed a macrocrack that had only partially propogated through their cross-section. A study was made of a few of these particular specimens.

Due to the fact that each specimen had been subjected to a large number of cycles, the macrocracks exhibited extensive deformation and fretting of the fracture surfaces. From the specimens studied, it was concluded that the macrocracks were transcrystalline in nature for specimens fatigued at stress amplitudes of ± 12.7, ± 13.0, ± 14.0 ksi. Specimens fatigued at a stress amplitude of ± 16.5 ksi were still characterized by predominantly transcrystalline

macrocracks but had some sections of an intercrystalline failure mode. All these macrocracks were within the endurance range of Stage II Crack propogation (Ref. 20).

Careful electropolishing revealed several crack tip features. The macrocrack was oriented at 90° to the stress axis, which is vertical in Figs. 42-46. (Stage II Crack propogation). The plastic relaxation process as reported by Laird (Ref. 20) is confirmed in Figs. 42-46. Figure 42 shows a crack after $8.179(10)^5$ cycles that has been left in the compression part of the loading cycle. Areas of deformation can be seen in front of and alongside the crack. Juxtaposed depressions can be observed on both fracture surfaces. Figure 43 shows the same macrocrack but unetched. The branch crack that lies at 45° to the main crack direction is thought to be an effect of Plastic deformation, rather than due to quasi-cleavage. It appears not to have been a rest point for the crack. Figure 44 gives an enlarged view of the crack tip of Figs.42 and 43. This picture clearly shows the asymmetrical notch left at the crack tip in compression. A crack tip in tension after $1.042(10)^6$ cycles is shown in Fig. 45. Figure 46 shows the same crack tip after re-polishing. It should be noted that the width of this crack is appreciably larger than the crack under the compression part of the cycle shown in Fig. 44. Figures 44 and 45 are both at 1000X magnification.

IV. CONCLUDING REMARKS

The availability of an extremely large number of fatigued specimens from which to select those for metallurgical investigation resulted in arriving at a fairly definitive picture of the microstructural damage at a particular stress amplitude. The microstructural evidence shows that the fatigue mechanism responsible for failure are H and F and the observed transition from H to F suggests the co-existance of both fatigue mechanisms. At all stress amplitudes, within the limits of observational and interpretive error, the percentages of H and F range microstructure were found to agree quite closely with the percentages of the STF and LTF fractions of the apparent bimodal endurance distributions of Ref. 15.

The initial work-hardened surface layer revealed microcracks after fatiguing which were initiated by the lathe tool pressure and originated at the roots of the grooves. Some spalling was observed at the interface between the cold-worked surface layer and the annealed core. This cold-worked layer blocked the F zones forming in the core from reaching the free surface and opening up into microcracks. However, some F zones ultimately must get through this layer, either directly or by linking with more irregular H-type microcracks which start in the layer itself preferentially at the roots of the tool grooves. It seems that in general the observed F zone blocking effect could be beneficial as far as fatigue life is concerned, although it is likely to accentuate the scatter in life.

Re-annealed and electropolished specimens revealed the typical core and surface features as reported by Wood (Ref. 3) for the same, but properly annealed, material under alternating torsion. Examination of the electropolished surface demonstrated the concentrated slip and fatigued slip bands that have been widely reported in the literature. At points of high stress concentration in the vicinity of the macrocrack of specimens fatigued at a stress amplitude of $\pm$ 12 ksi., the crystallite and kink band formation on the

surface, reported by Forsyth (Ref. 17) as typical for specimens fatigued at higher stress amplitudes, was observed.

Macrocracks examined in specimens fatigued at stress amplitudes of $\pm$ 12.7, $\pm$ 13 and $\pm$ 14 ksi were all found to be transcrystalline in nature. Specimens fatigued at a stress amplitude of $\pm$ 16.5 ksi exhibited predominantly transcrystalline cracks with some evidenc of intercrystalline failure.

Particular specimens in which the crack tip was visible confirmed the features of the plastic relaxation process of crack tip formation reported by Laird (Ref. 20).

REFERENCES

1. Manson, S.S. — NACA Report No. 1170, 1954
2. Coffin, L.F., Jr. — Trans. AIME, Vol. 76, 1954
3. Wood, W.A. — Experimental Approach to Basic Study of Fatigue, Institute for the Study of Fatigue and Reliability Report No. 24, Columbia University, August, 1965.
4. Williams, T.R.G. — The Extrusion Characteristics and Mechanical Properties of Aluminum Alloy L-65, AASU Report No. 189, August 1961.
5. Lowcock, M.T. Williams, T.R.G. — Effect of Random Loading on the Fatigue Life of Aluminum Alloy L-73, AASU Report No. 225, July 1962.
6. Shabalin, V.I. — Discontinuity in the Fatigue Curve for Duralumin, Metal Industry, Jan. 1959.
7. Gill, P.A.T. — M.Sc. Thesis, Southampton University, 1963.
8. Swanson, S.R. — An Investigation of the Fatigue of Aluminum Due to Random Loading, UTIA Report No. 84, 1963.
9. Porter, J. Levy, J.C. — The Fatigue Curves of Copper, Journal of the Institute of Metals, Vol. 89, 1960-61.
10. Nine, H.D. — Discontinuities in the S-N Fatigue Curve of <111> Copper Single Crystals, Trans. AIME, Vol. 233, July 1965.
11. Nine, H.F. Bendler, H.M. — Effect of Strain Amplitude on Fatigue in Copper Single Crystals, ACTA Met. Vol. 12, August 1964.
12. Benham, P.P. Ford, H. — J. Mech. Eng. Sci., Vol. 3, 1961.
13. Cicci, F. — An Investigation of the Statistical Distribution of Constant Amplitude Fatigue Endurances for a Maraging Steel, UTIA Technical Note No. 73, July, 1964.
14. Frost, N.E. — Difference Between High- and Low-Stress Fatigue, Nature, Vol. 192, 1961.
15. Haagenson, P.J. — UTIAS Technical Note No. 112 (to be published)
16. Averbach et al, B.L. (ed.) — Fracture, John Wiley and Sons, 1959.
17. Forsyth, P.J.E. — Some Metallographic Observations on the Fatigue on Metals, Jour. of the Institute of Metals, Vol. 80, 1951-1952.

18. Kemsley, D. S. The Behaviour of Cold-Worked Copper in Fatigue. Journal of the Institute of Metals, Vol. 87, 1958-59.

19. Mott, N.F. Acta Met., Vol. 6, p. 195, 1958.

20. Laird, C. The Influence of Metallurgical Structure on the Mechanism of Fatigue Crack Propogation, Symposium on Fatigue Crack Propogation, ASTM STP 32, June 1966.

TABLE I

CONTROL TENSILE SPECIMEN DATA

Specimen Designation	Diameter (Mean) (inches)	0.2% Proof Stress (psi)	Tensile Strength (psi)	$E \times 10^{-6}$ (psi)	Elongation on 1 in. (%)	Area Reduction (%)	Diamond Pyramid Hardness of Unfatigued Material
* A-1	.292	6,934	40,726	15.96	65.0	92.0	41.4
A-2	.292	9,084	40,574	18.00	59.8	92.0	40.0
A-3	.292	10,598	41,180	15.95	61.7	92.0	40.5
A-4	.292	7,873	40,877	16.20	62.9	92.4	39.0
A-5	.291	7,645	40,574	17.90	63.5	92.0	39.5
A-6	.292	8,418	40,271	17.90	65.0	92.4	39.4
A-7	.291	7,645	40,271	17.13	64.5	92.2	39.6
B-1	.292	10,053	40,877	16.93	59.3	91.8	44.6
B-2	.291	8,175	40,574	17.43	60.0	92.0	42.2
B-3	.291	9,190	40,423	16,86	59.3	92.0	42.4
B-4	.291	8,281	40,726	17.85	59.4	91.8	43.9
B-5	.292	8,705	40.271	17.27	59.7	92.6	42.4
B-6	.292	9,493	40,877	17.20	60.0	91.8	43.1
B-7	291	9,356	40,276	17.10	59.1	92.6	44.6
C-1	.292	10,885	40,877	16.60	61.7	92.6	44.4
C-2	.292	9,417	40,877	17.40	60.4	92.0	43.9
C-3	.292	9,538	41,180	16.70	62.1	92.6	44.7
C-4	.291	10,219	40,574	16.60	61.8	92.4	43.9
C-5	.292	9.614	40,574	16.85	60.1	91.8	41.6
C-6	.292	8,705	40.877	16.75	61.6	91.8	41.7
D-1	.291	10,355	41,028	17.96	61.7	92.4	43.2
D-2	.292	9,992	41,028	17.56	62.5	91.6	42.4
D-3	.291	7,797	41,331	18.12	61.7	92.4	42.5
D-4	.291	9,311	40,877	17,63	62.5	91.6	42.4
D-5	.291	7,479	40,574	18,68	61.2	91.6	41.8
D-6	.292	8,327	41,180	18.60	61.7	92.0	41.1
D-7	.292	9,508	41,331	17.93	60.7	92.0	42.0
Mean		8,899	40,790	17.30	61.4	92.1	42.2
Standard Deviation		1,042	306	0.73			
95% Confidence Limits		8,490 9,308	40,670 40,910	17.01 17.59			

* Letter designates Heat treatment batch.

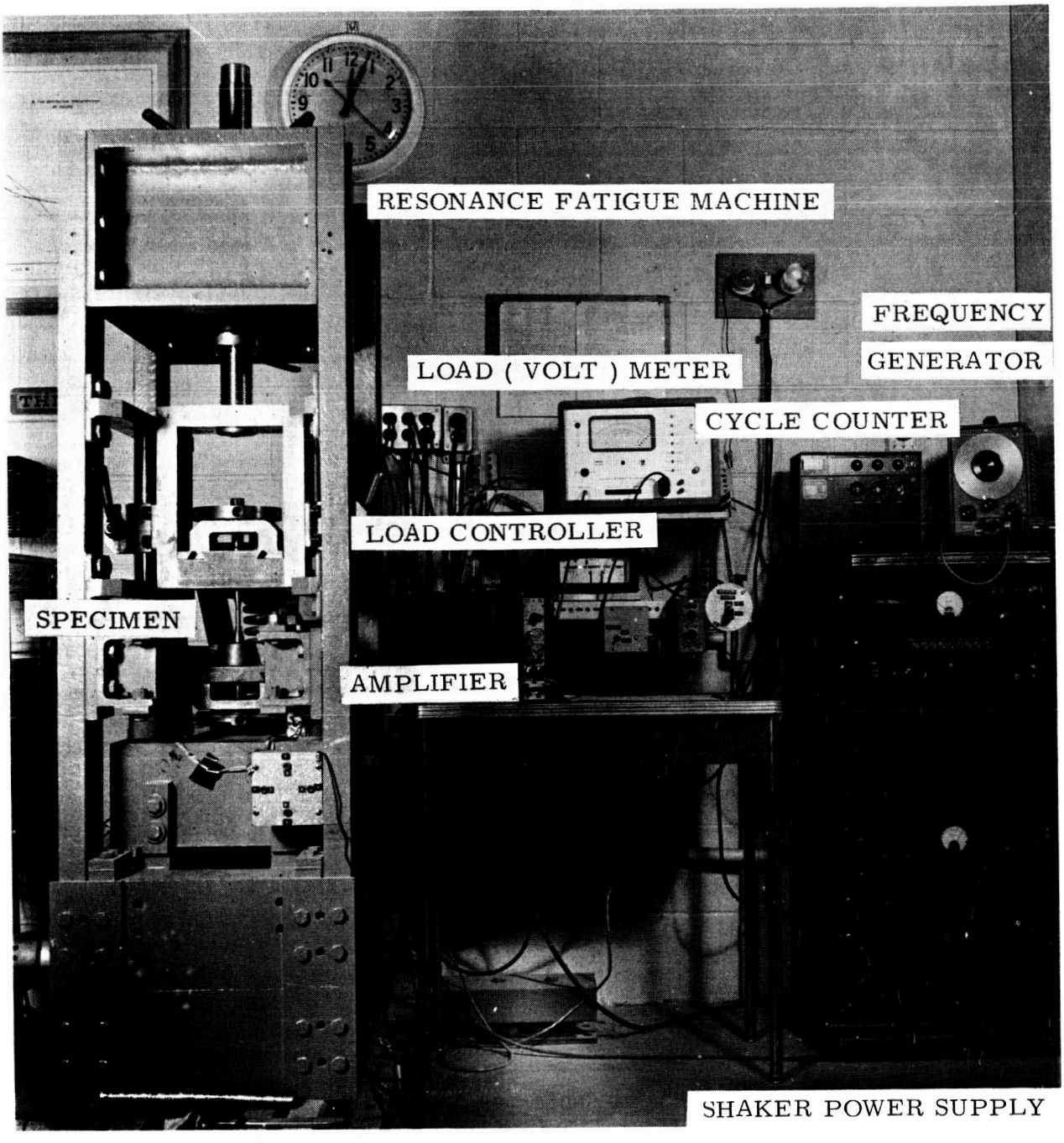

FIG. 1. TEST APPARATUS.

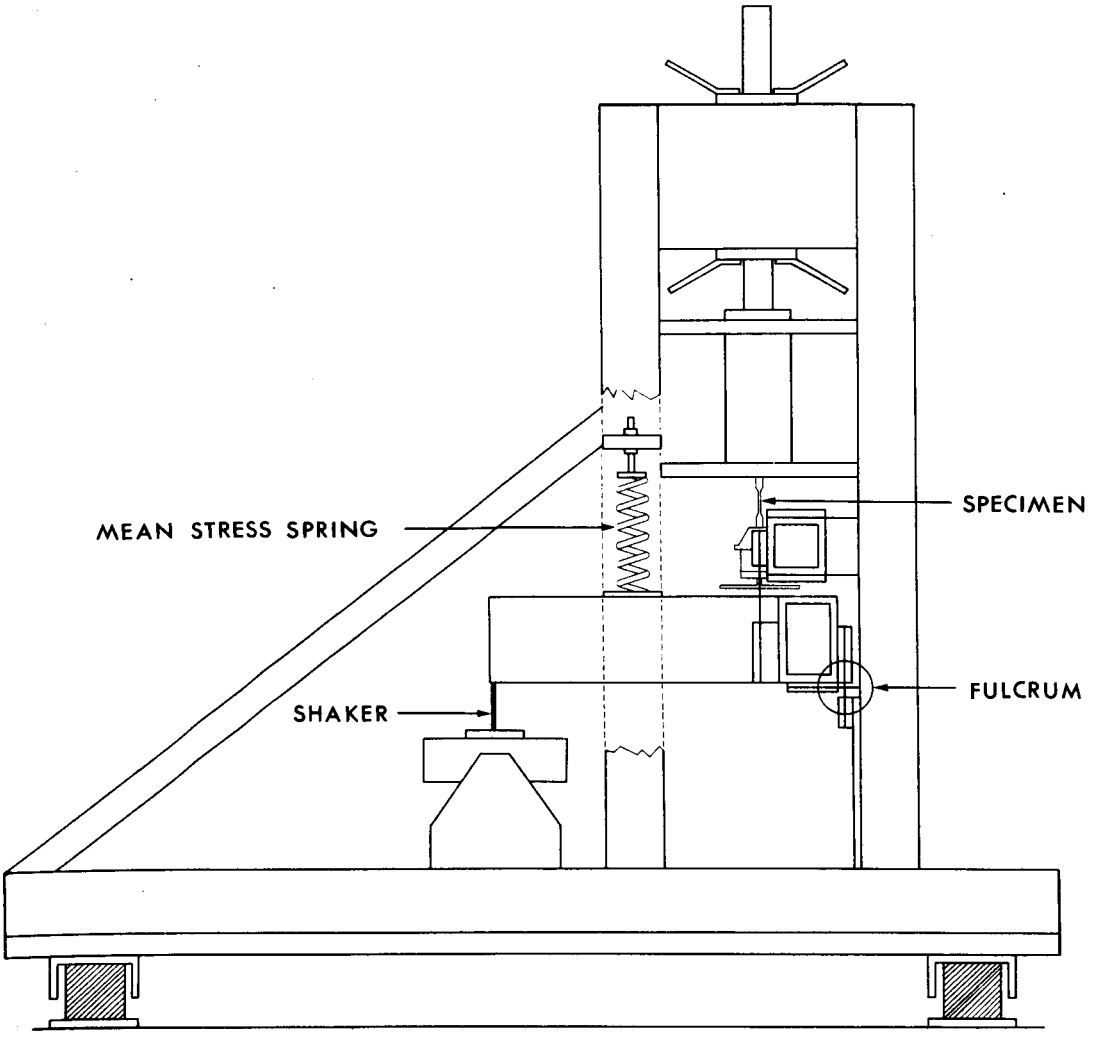

FIG. 2 SCHEMATIC LAYOUT OF FATIGUE TESTING MACHINE

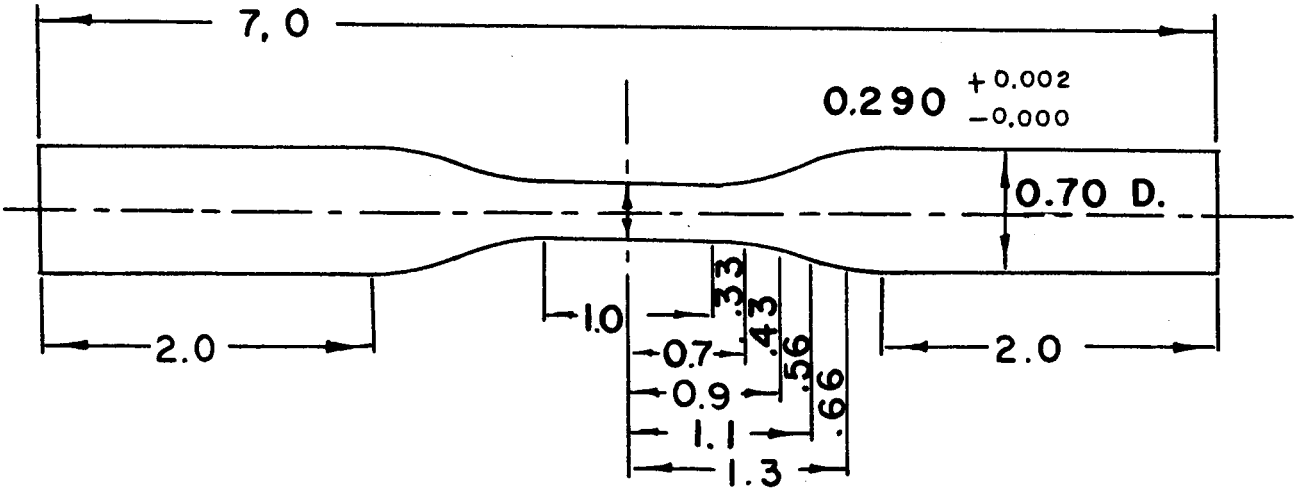

FIG. 3. THE COPPER (O. F. H. C.) FATIGUE SPECIMEN.

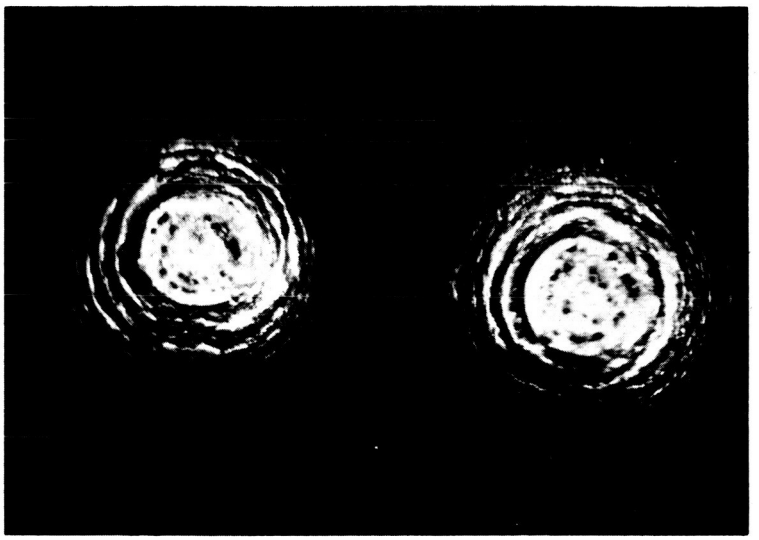

FIG. 4 "DOUBLE CUP" TENSILE FRACTURE. (x 15).

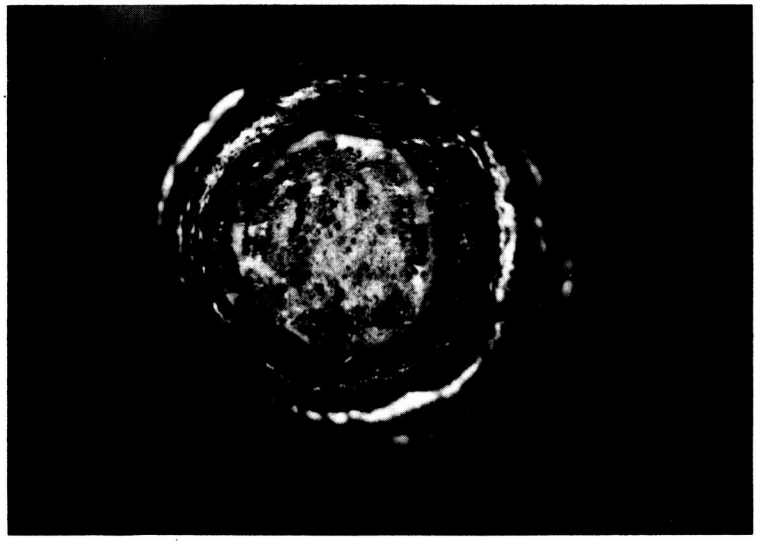

FIG. 5 FRACTURE SURFACE OF ONE HALF OF SPECIMEN SHOWN IN FIG. 4. NOTE CAVITIES ON BASE OF DUCTILE CUP FRACTURE. (x 30).

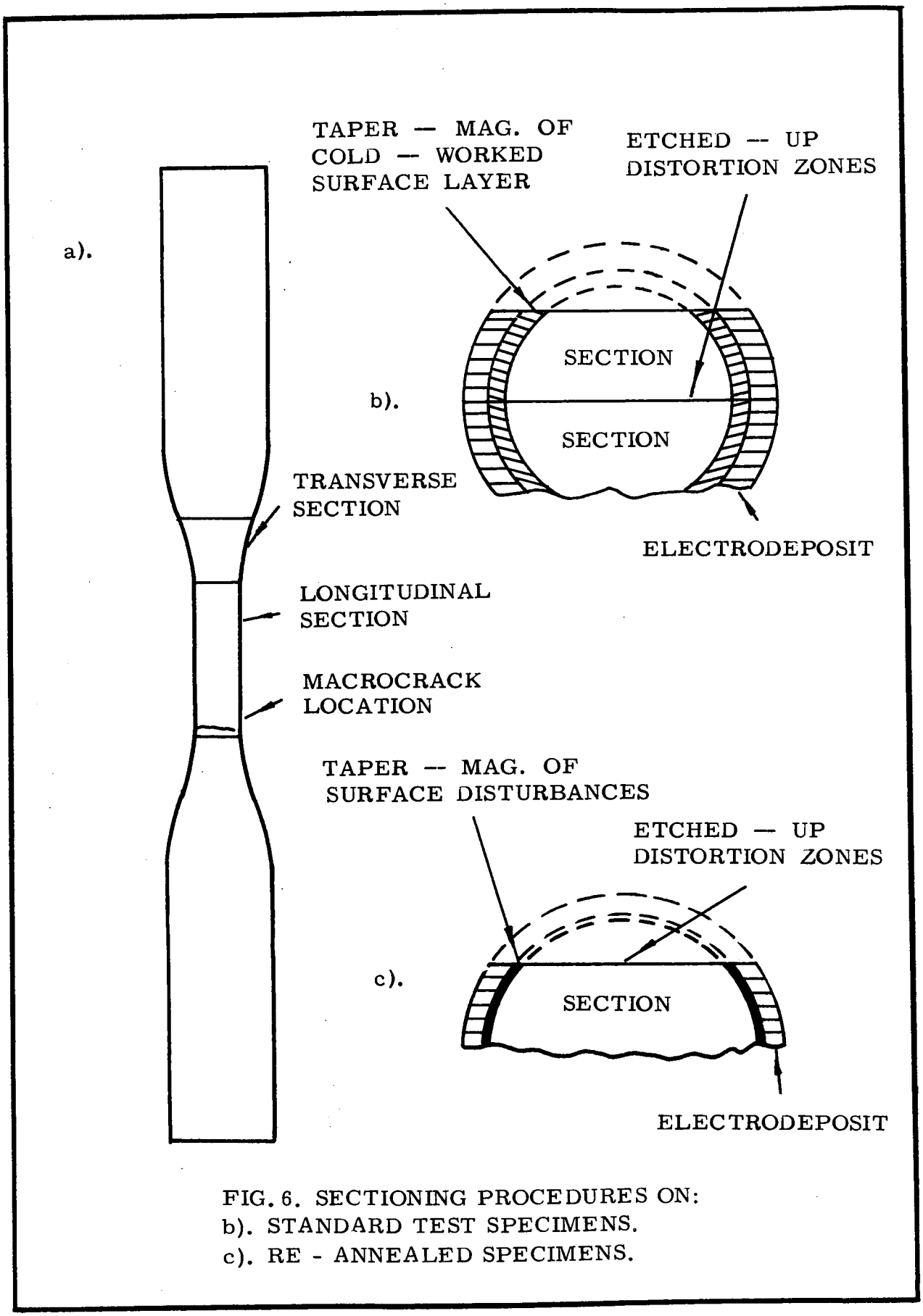

FIG. 6. SECTIONING PROCEDURES ON:
b). STANDARD TEST SPECIMENS.
c). RE - ANNEALED SPECIMENS.

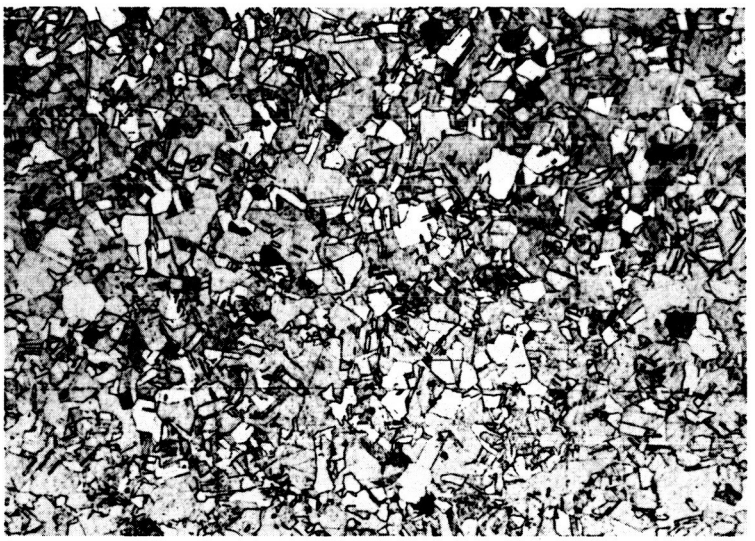

FIG. 7 TYPICAL TRANSVERSE SECTION OF SPECIMEN BEFORE FATIGUING. A. S. T. M. GRAIN SIZE NO. 8. 0. (x 100).

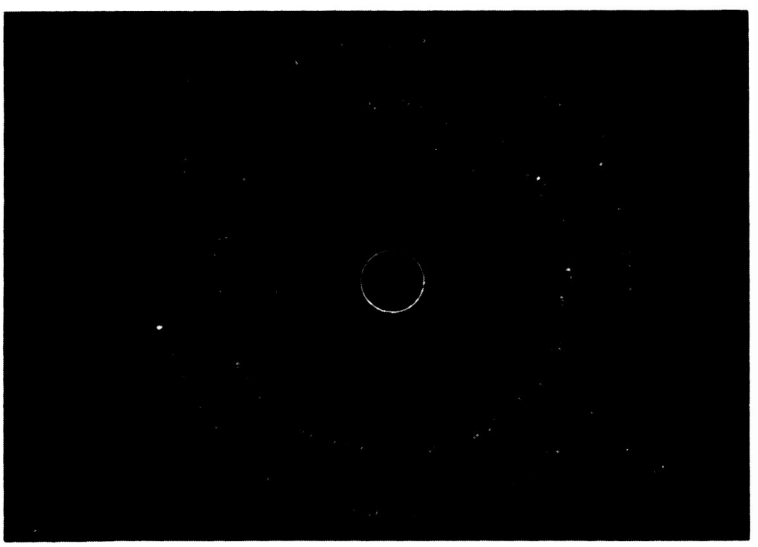

FIG. 8 X-RAY BACK-REFLECTION PATTERN OF CORE OF LONGITUDINAL SPECIMEN BEFORE FATIGUING (Cu. radiation).

FIG. 9 TYPICAL VIEW OF SURFACE OF SPECIMEN FROM HEAT TREATMENT BATCH A. SURFACE GROOVES ARE LEFT BY FINE-MACHINING AFTER ANNEALING. (x 200).

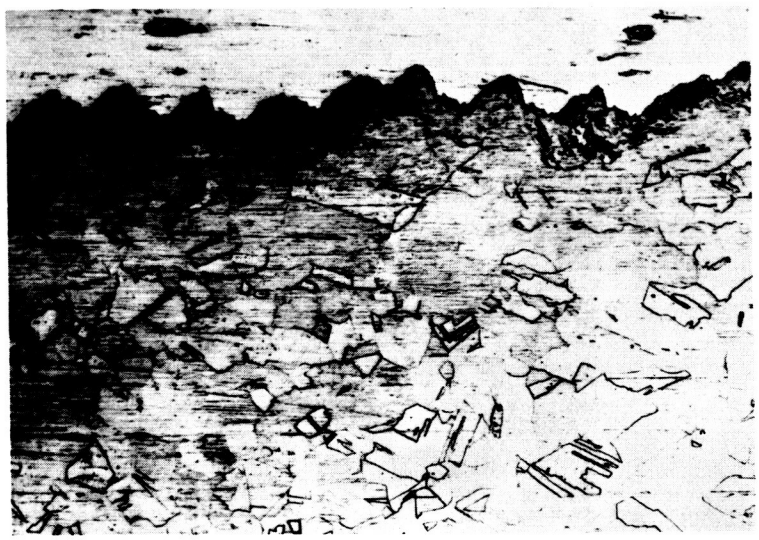

FIG. 10 TYPICAL VIEW OF SURFACE OF SPECIMEN FROM HEAT TREATMENT BATCH C. SURFACE GROOVES ARE LEFT BY FINE-MACHINING AFTER ANNEALING. (x 200).

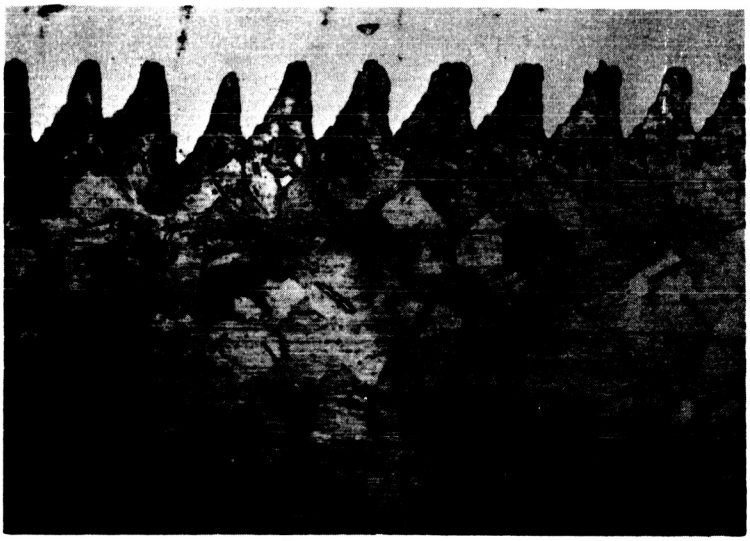

FIG. 11 TYPICAL VIEW OF SURFACE OF SPECIMEN FROM HEAT TREATMENT BATCH B. SURFACE GROOVES ARE LEFT BY FINE-MACHINING AFTER ANNEALING. (x 200).

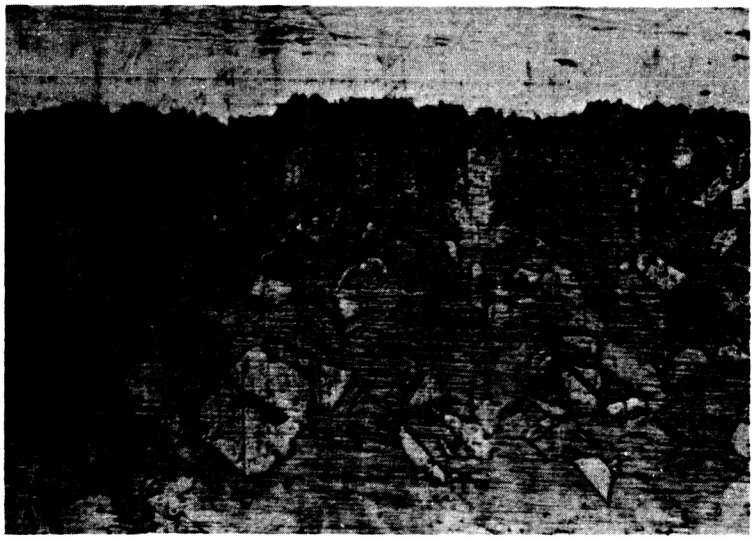

FIG. 12 TYPICAL VIEW OF SURFACE OF SPECIMEN FROM HEAT TREATMENT BATCH D. SURFACE GROOVES LEFT BY FINE-MACHINING TOOL HAVE SUBSEQUENTLY BEEN RUBBED DOWN WITH EMERY PAPER. (x 200).

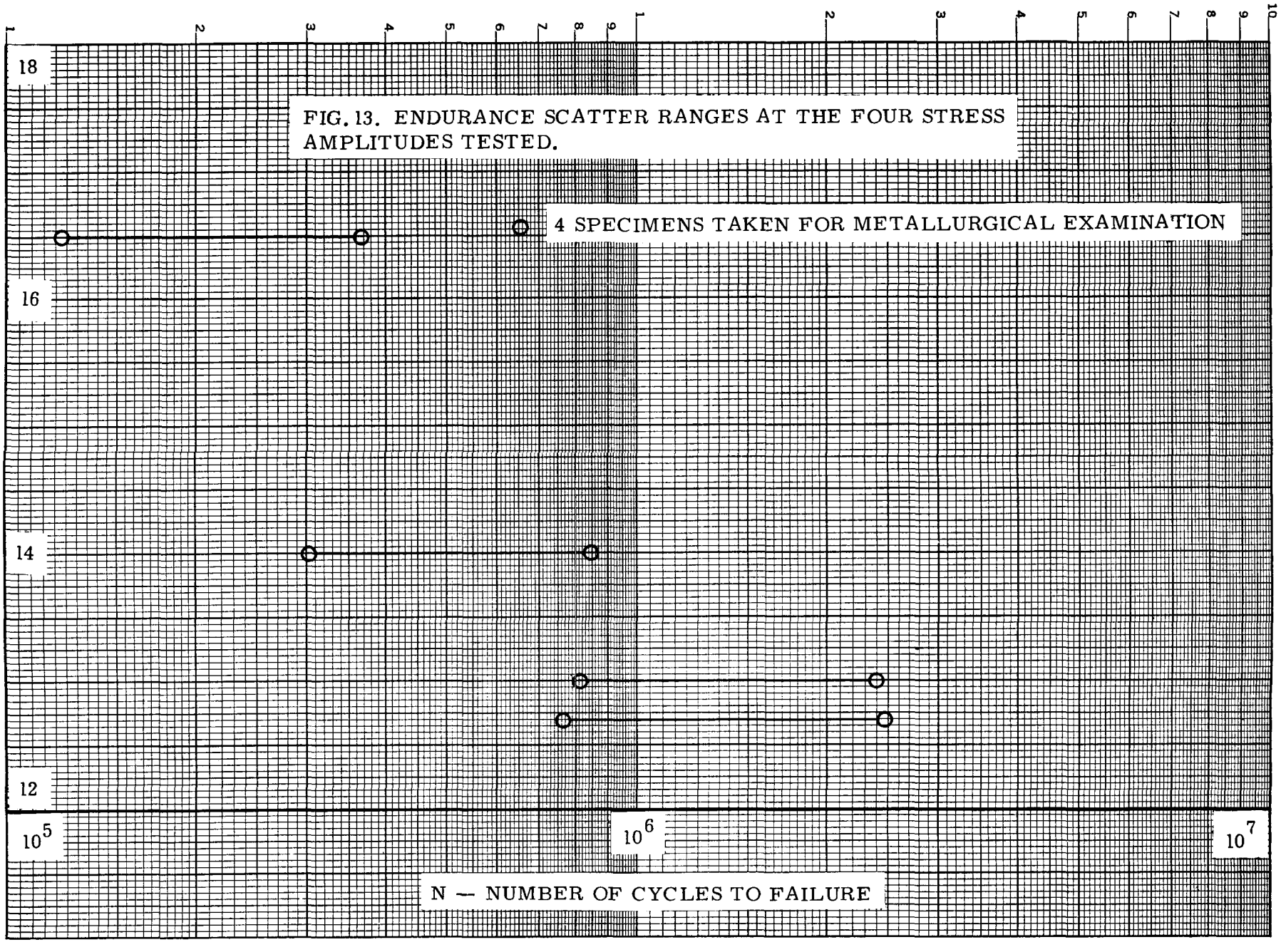
FIG. 13. ENDURANCE SCATTER RANGES AT THE FOUR STRESS AMPLITUDES TESTED.
4 SPECIMENS TAKEN FOR METALLURGICAL EXAMINATION
S — ALTERNATING STRESS AMPLITUDE (k.s.i.)
18
16
14
12
10^5
10^6
10^7
N — NUMBER OF CYCLES TO FAILURE

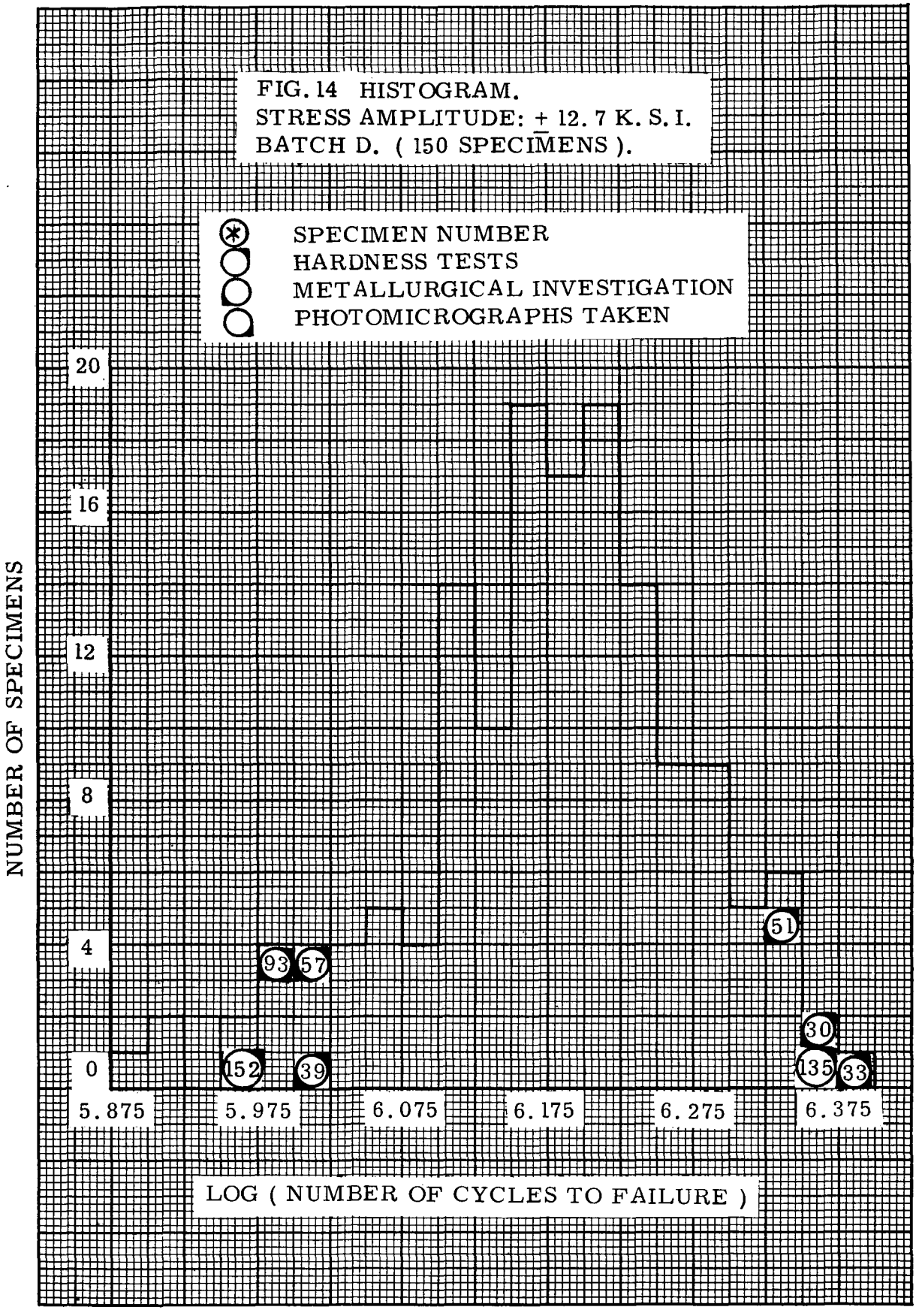
FIG. 14 HISTOGRAM.
STRESS AMPLITUDE: + 12.7 K.S.I.
BATCH D. (150 SPECIMENS).
SPECIMEN NUMBER
HARDNESS TESTS
METALLURGICAL INVESTIGATION
PHOTOMICROGRAPHS TAKEN
NUMBER OF SPECIMENS
20
16
12
8
4
0
93
57
51
30
152
39
135
33
5.875
5.975
6.075
6.175
6.275
6.375
LOG (NUMBER OF CYCLES TO FAILURE)

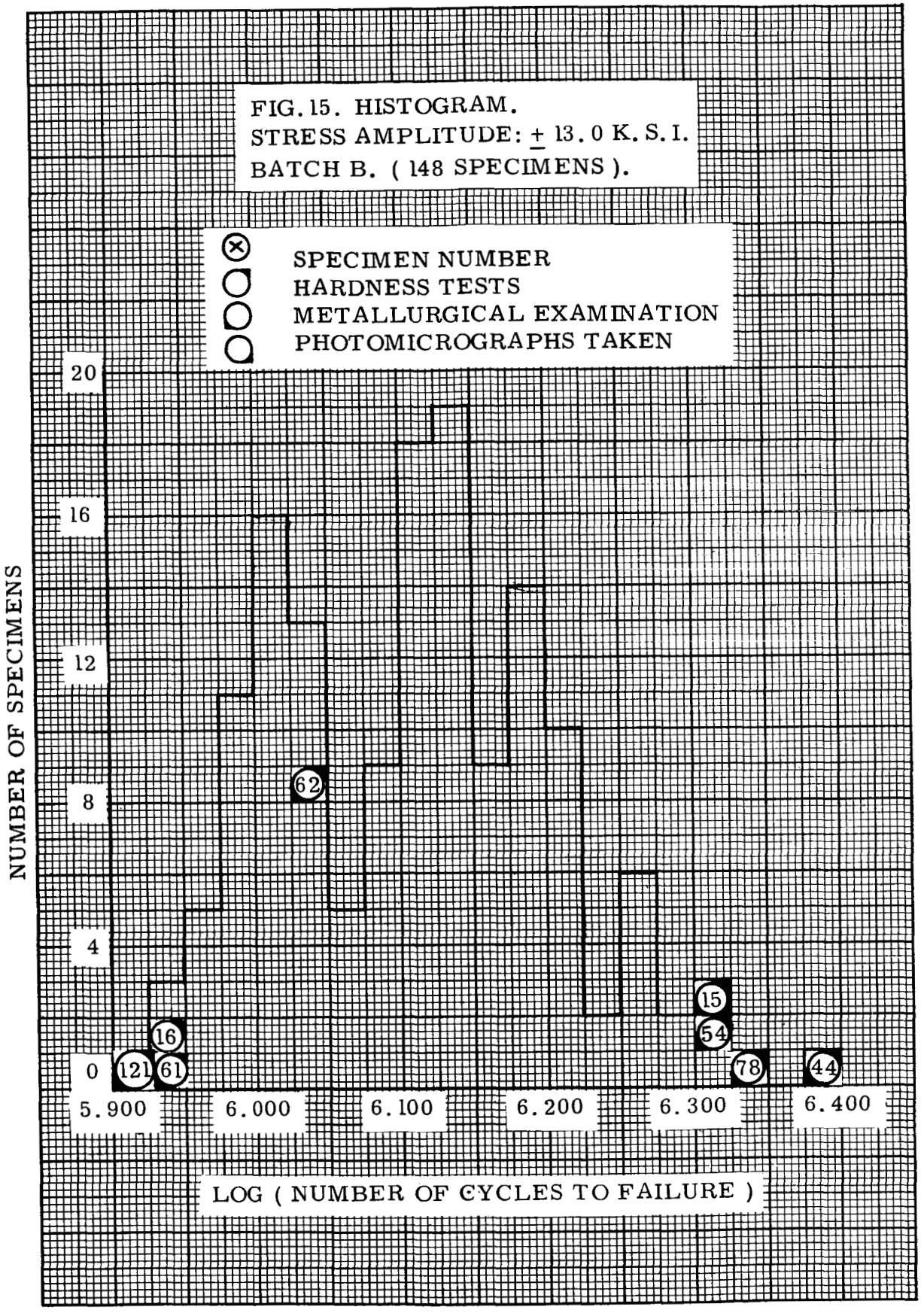
FIG. 15. HISTOGRAM.
STRESS AMPLITUDE: ± 13.0 K.S.I.
BATCH B. (148 SPECIMENS).
SPECIMEN NUMBER
HARDNESS TESTS
METALLURGICAL EXAMINATION
PHOTOMICROGRAPHS TAKEN
NUMBER OF SPECIMENS
20
16
12
8
4
0
62
15
54
16
121
61
78
44
5.900
6.000
6.100
6.200
6.300
6.400
LOG (NUMBER OF CYCLES TO FAILURE)

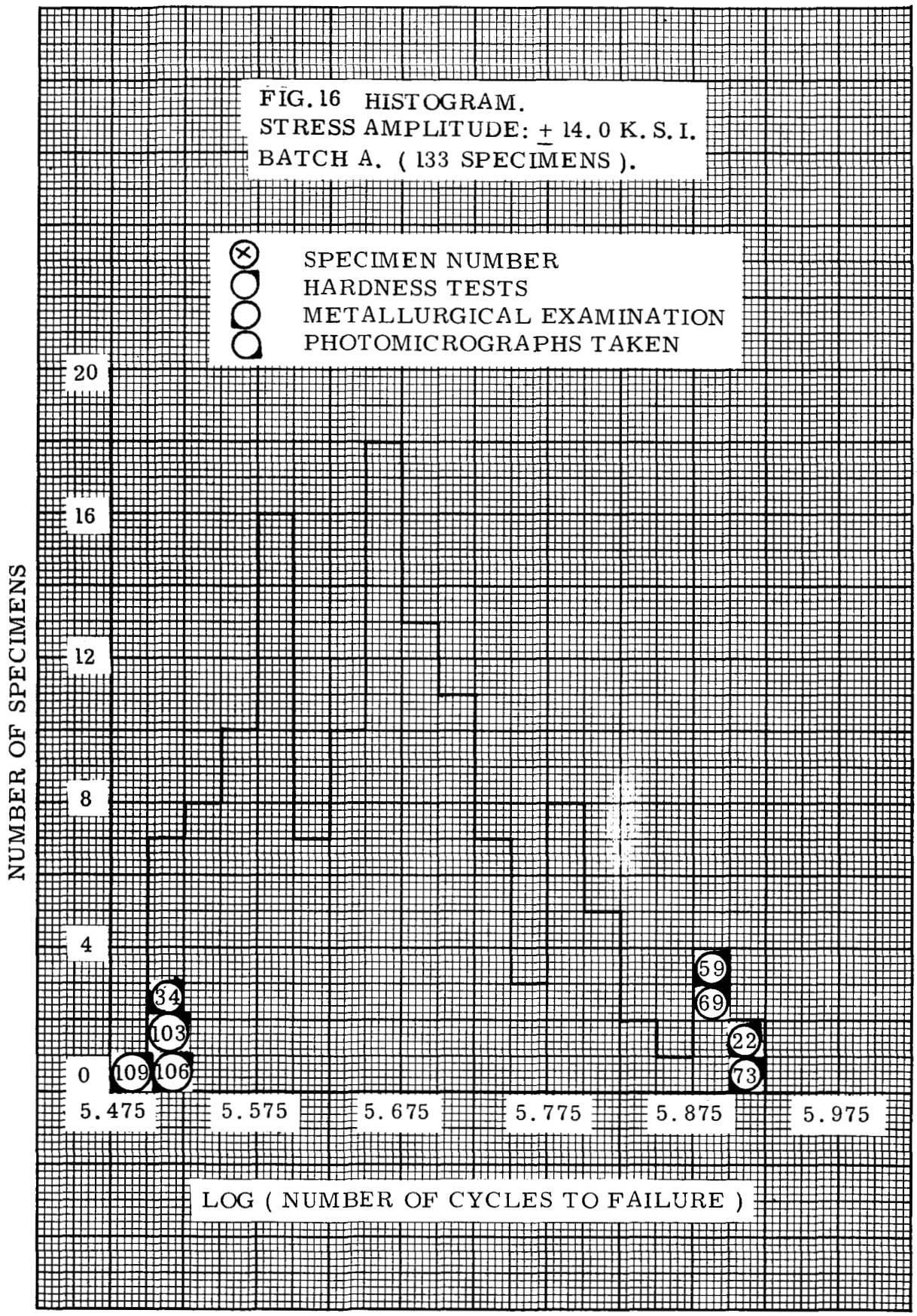
FIG. 16 HISTOGRAM.
STRESS AMPLITUDE: ± 14.0 K.S.I.
BATCH A. (133 SPECIMENS).
SPECIMEN NUMBER
HARDNESS TESTS
METALLURGICAL EXAMINATION
PHOTOMICROGRAPHS TAKEN
NUMBER OF SPECIMENS
20
16
12
8
4
0
34
103
109
106
59
69
22
73
5.475
5.575
5.675
5.775
5.875
5.975
LOG (NUMBER OF CYCLES TO FAILURE)

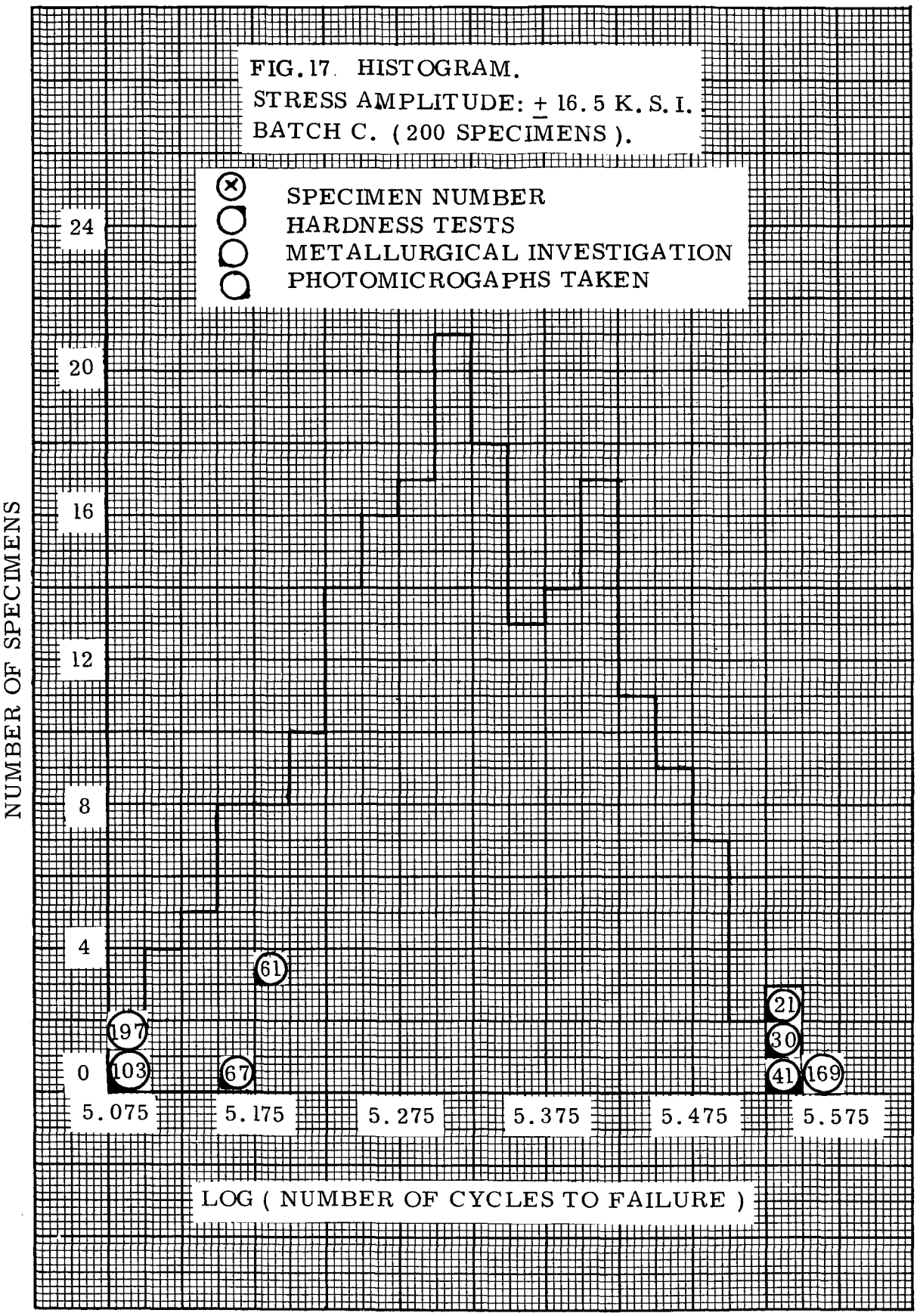
FIG. 17 HISTOGRAM.
STRESS AMPLITUDE: ± 16.5 K.S.I.
BATCH C. (200 SPECIMENS).
SPECIMEN NUMBER
HARDNESS TESTS
METALLURGICAL INVESTIGATION
PHOTOMICROGAPHS TAKEN
NUMBER OF SPECIMENS
24
20
16
12
8
4
0
61
197
103
67
21
30
41
169
5.075
5.175
5.275
5.375
5.475
5.575
LOG (NUMBER OF CYCLES TO FAILURE)

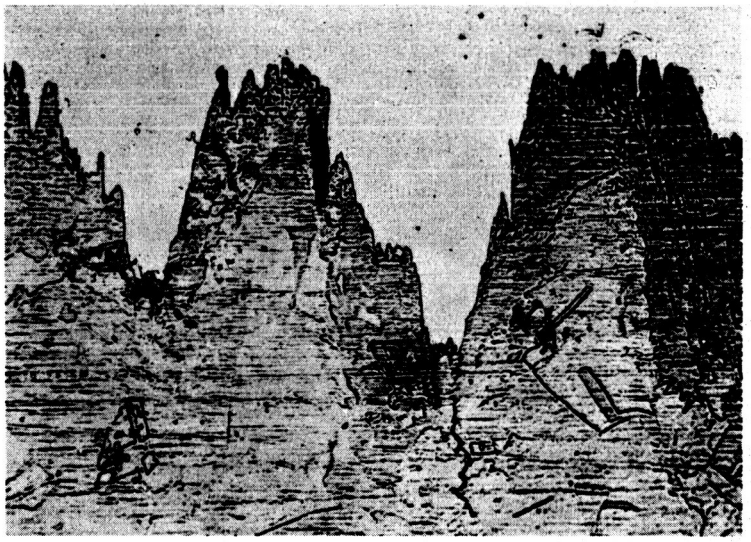

FIG. 18 MICROCRACK DEVELOPING AT ROOT OF GROOVE LEFT BY FINE-MACHINING TOOL. (A-34, $\pm$ 14 ksi, x 500).

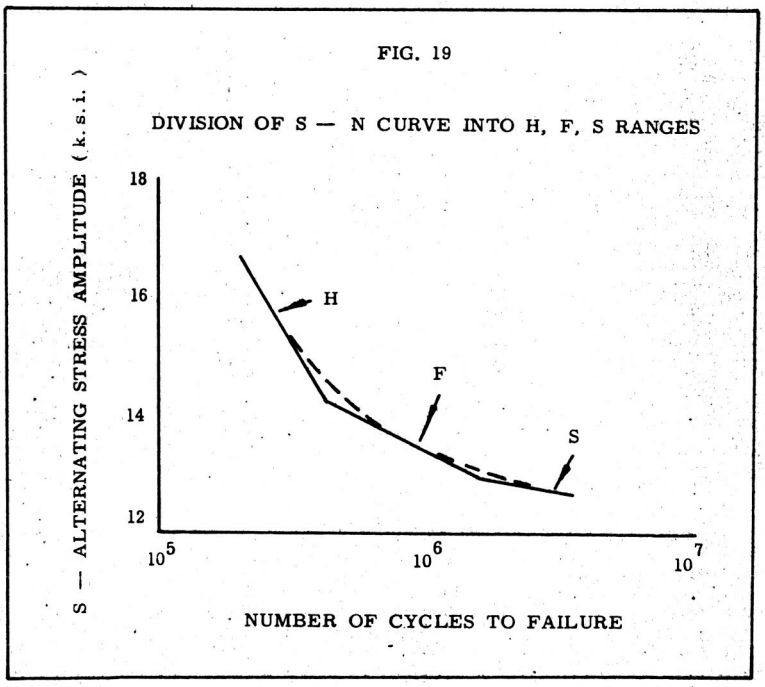

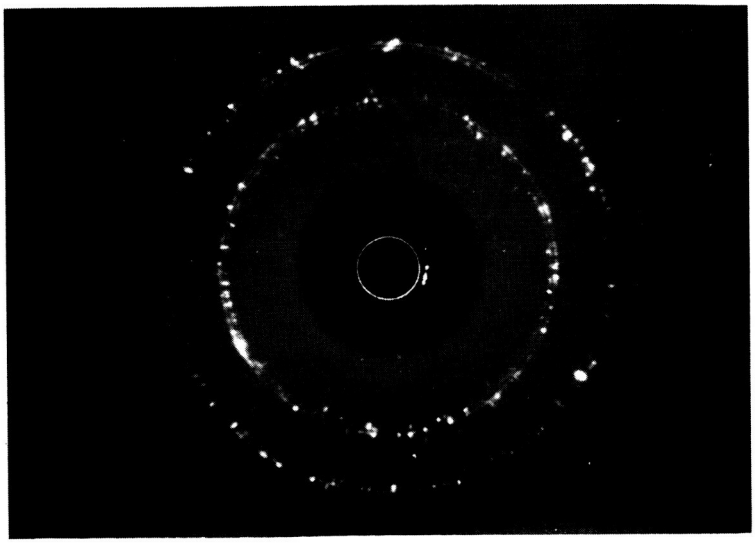

FIG. 20 X-RAY BACK-REFLECTION PATTERN OF SPECIMEN FATIGUED AT A STRESS AMPLITUDE OF $\pm$ 12.7 ksi. (Cu. radiation).

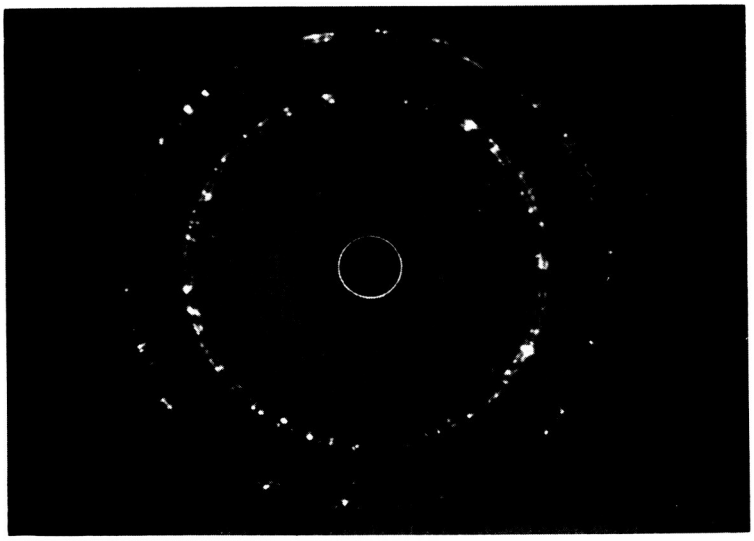

FIG. 21 X-RAY BACK-REFLECTION PATTERN OF SPECIMEN FATIGUED AT A STRESS AMPLITUDE OF $\pm$ 13.0 ksi. (Cu. radiation).

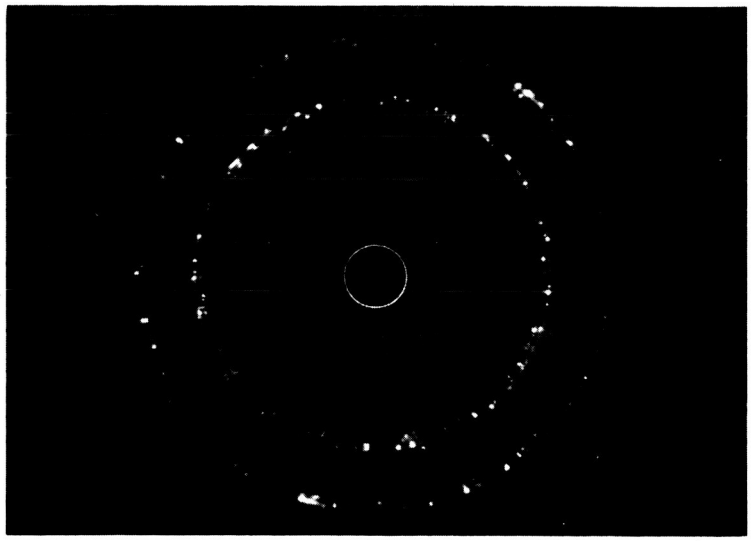

FIG. 22 X-RAY BACK-REFLECTION PATTERN OF SPECIMEN FATIGUED AT A STRESS AMPLITUDE OF $\pm$ 14.0 ksi. (Cu. radiation).

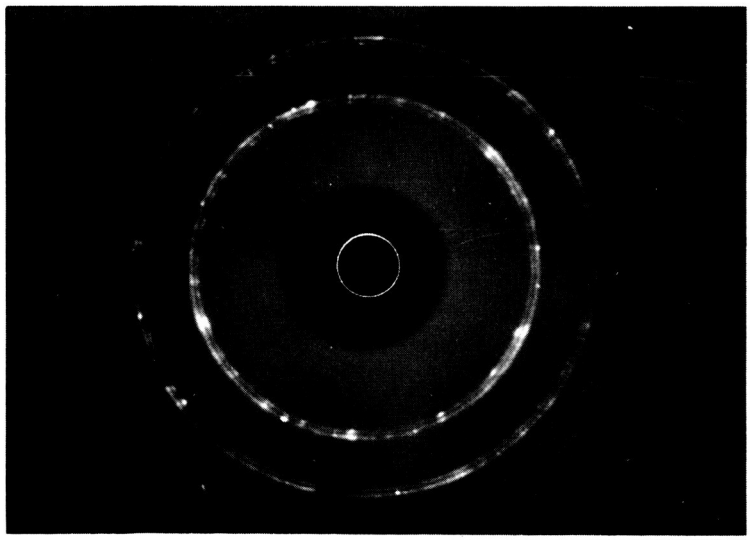

FIG. 23 X-RAY BACK-REFLECTION PATTERN OF SPECIMEN FATIGUED AT A STRESS AMPLITUDE OF $\pm$ 16.5 ksi. (Cu. radiation).

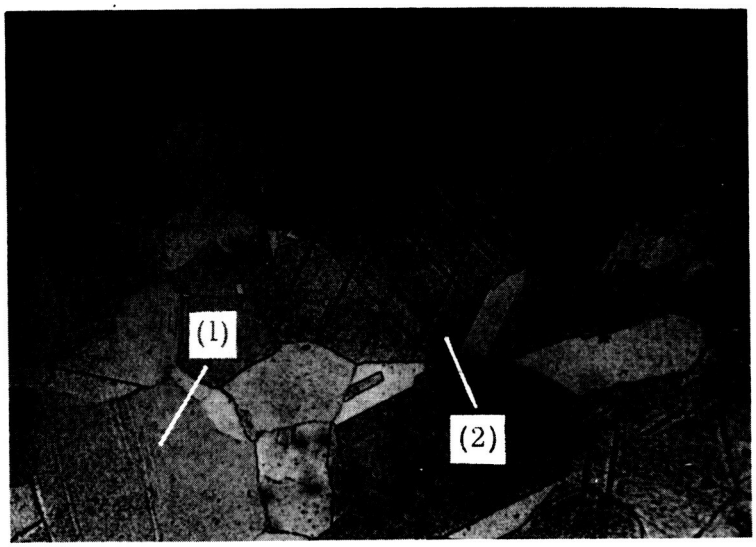

FIG. 24 CROSS SLIP AND TYPICAL F RANGE DAMAGE. (D-93, $\mp$ 12.7 ksi, x 500).

1. DISTORTED SLIP-ZONES

2. CROSS SLIP

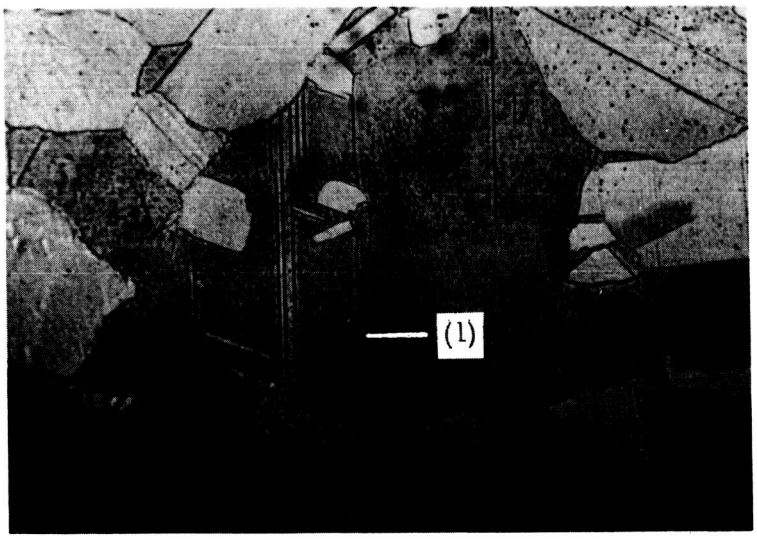

FIG. 25 ETCHED-UP FATIGUED SLIP-ZONES. (D-93, $\pm$ 12.7 ksi, x 500).

1. DISTORTED SLIP-ZONES

FIG. 26 ETCHED SECTION. DISTORTED SLIP-ZONES, SOME H RANGE MICROSTRUCTURE AND GRAIN BOUNDARY DAMAGE. (B-15, ± 13.0 ksi, x 500).

1. DISTORTED SLIP-ZONES

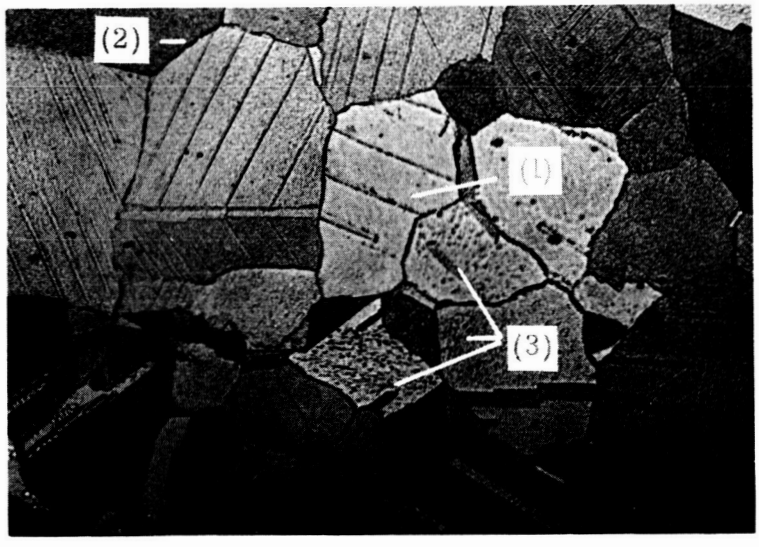

FIG. 27 ETCHED SECTION. FATIGUED SLIP-ZONES, SOME H RANGE STRUCTURE. GRAIN BOUNDARY DAMAGE. (A-59, ± 14.0 ksi, x 500).

1. FATIGUED SLIP-ZONES

2. GRAIN BOUNDARY DAMAGE

3. H RANGE DAMAGE

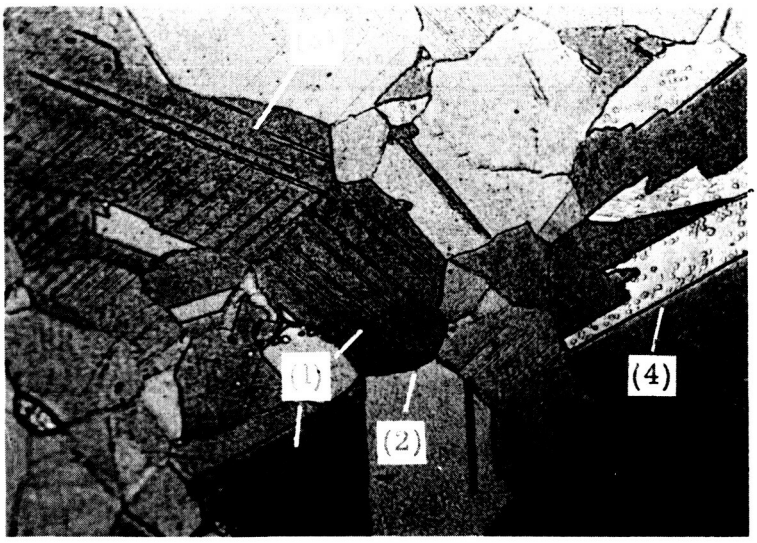

FIG. 28 ETCHED SECTION. DISTORTED SLIP-ZONES AND CROSS SLIP. DEFORMATION OF TWIN BOUNDARIES. SOME H RANGE DAMAGE. (A-59, ± 14.0 ksi, x 500).

1. DISTORTED SLIP-ZONES

2. GRAIN BOUNDARY DAMAGE

3. CROSS SLIP

4. DISTORTION OF TWIN BOUNDARY

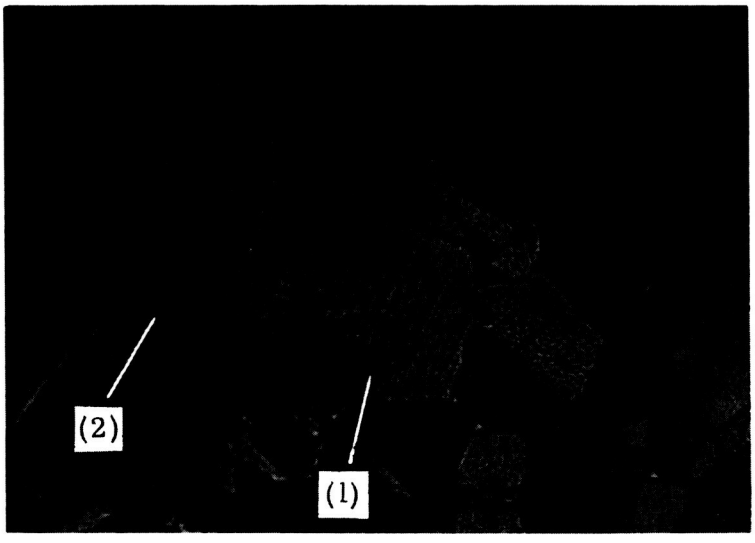

FIG. 29 FATIGUED SLIP-ZONES. DISORIENTED H RANGE DAMAGE. DAMAGE IN THE MIDDLE OF GRAIN EXHIBITING SLIP-ZONES. (C-41, ± 16.5 ksi, x 500).

1. FATIGUED SLIP-ZONES

2. DISTORTION DUE TO CROSS SLIP

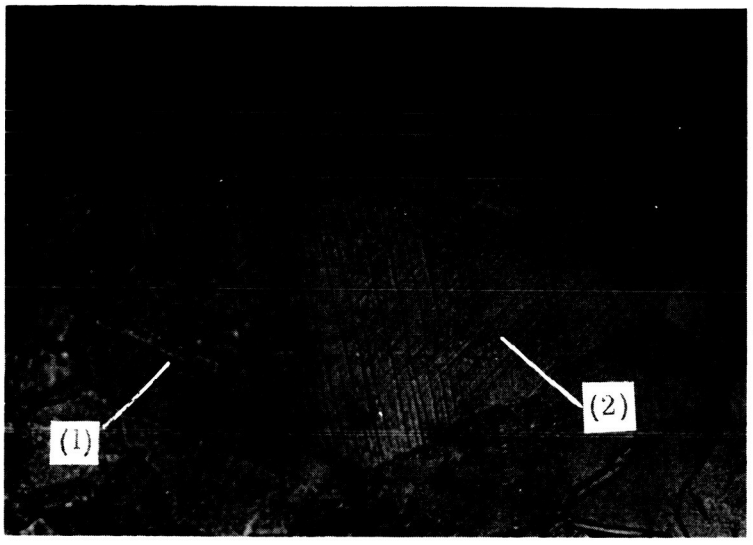

FIG. 30 ETCHED SECTION. CROSS SLIP. GRAIN AND CELL BOUNDARY DAMAGE. LARGE REGION OF CRYSTALLITE FORMATION. (C-41, ± 16.5 ksi, x 500).

1. TWIN BOUNDARY DISTORTION

2. CROSS SLIP

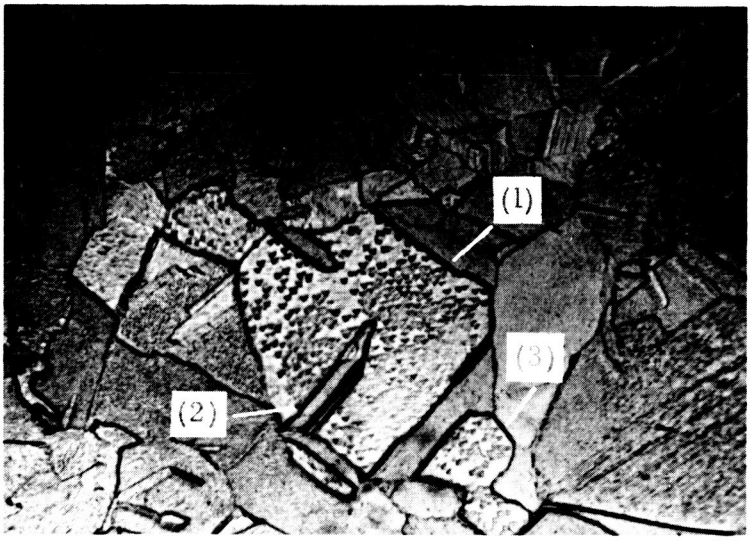

FIG. 31 TYPICAL DISORIENTED H RANGE STRUCTURE. GRAIN AND TWIN BOUNDARY DAMAGE. ETCH PITTS SHOW DISORIENTATION. SOME SLIP-ZONE DAMAGE. (C-41, ± 16.5 ksi, x 500).

1. ETCH PITTS

2. TWIN BOUNDARY DISTORTION

3. CELL BOUNDARY DAMAGE

FIG. 32 TWIN AND GRAIN BOUNDARY DAMAGE. FATIGUED SLIP-ZONES. (D-33, $\pm$ 12.7 ksi, x 500).

1. GRAIN BOUNDARY DAMAGE

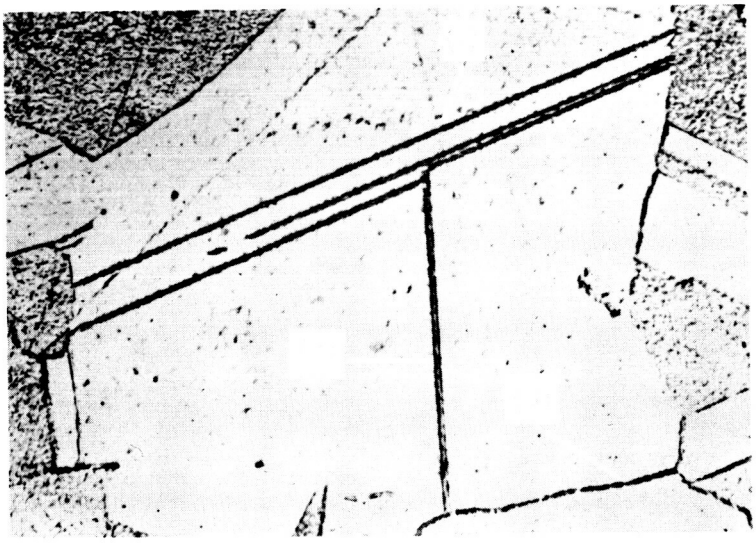

FIG. 33 FATIGUED SLIP-ZONES AND DAMAGE IN CROSS SLIP ZONE. GRAIN BOUNDARY DAMAGE. (D-33, $\pm$ 12.7 ksi, x 700).

1. FATIGUED SLIP-ZONES

2. CROSS SLIP

3. GRAIN BOUNDARY DAMAGE

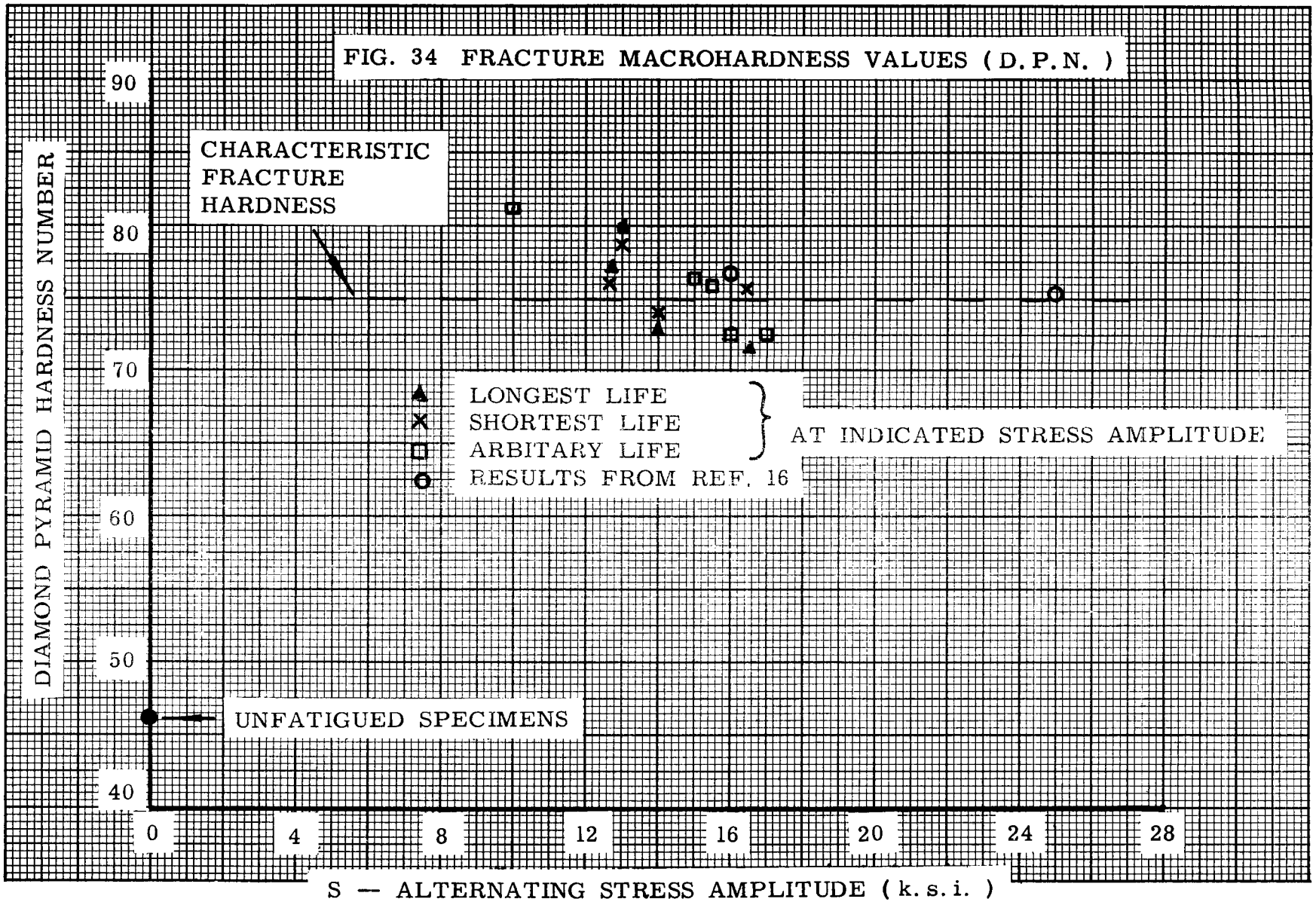
FIG. 34 FRACTURE MACROHARDNESS VALUES (D.P.N.)
DIAMOND PYRAMID HARDNESS NUMBER
90
80
70
60
50
40
CHARACTERISTIC FRACTURE HARDNESS
LONGEST LIFE
SHORTEST LIFE
ARBITARY LIFE
AT INDICATED STRESS AMPLITUDE
RESULTS FROM REF. 16
UNFATIGUED SPECIMENS
0
4
8
12
16
20
24
28
S — ALTERNATING STRESS AMPLITUDE (k.s.i.)

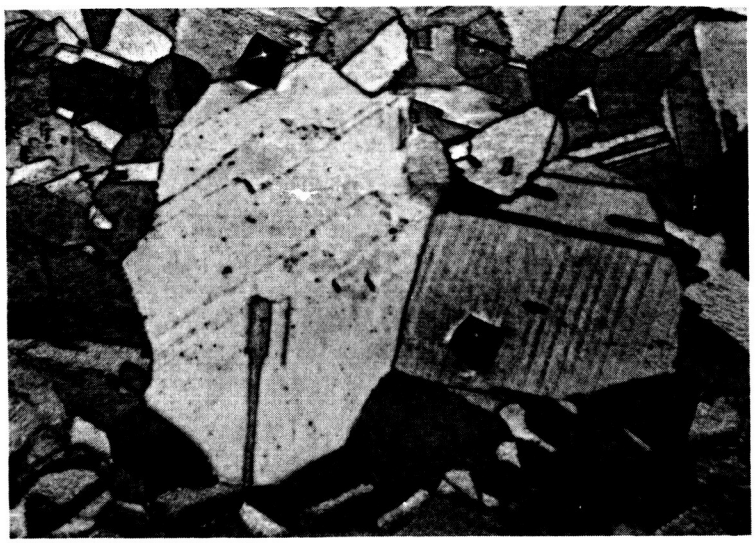

FIG. 35 TYPICAL VIEW OF MICROHARDNESS IMPRESSIONS. LOWER IMPRESSION PLACED IN A GRAIN EXHIBITING FATIGUED SLIP-ZONES. UPPER IMPRESSION PLACED ON BOUNDARY BETWEEN GRAINS SHOWING TWIN BOUNDARY DAMAGE. TOTAL FIELD SHOWS COEXISTENCE OF H AND F RANGE MICROSTRUCTURE. (C-41, $\pm$ 16.5 ksi, x 500). REDUCED 20% FOR PRINTING.

FIG. 36 TYPICAL LONGIDUDINAL SECTION OF RE-ANNEALED SPECIMEN. A.S.T.M. GRAIN SIZE NO. 4.0. (B-2R, $\pm$ 12.0 ksi, x 100).

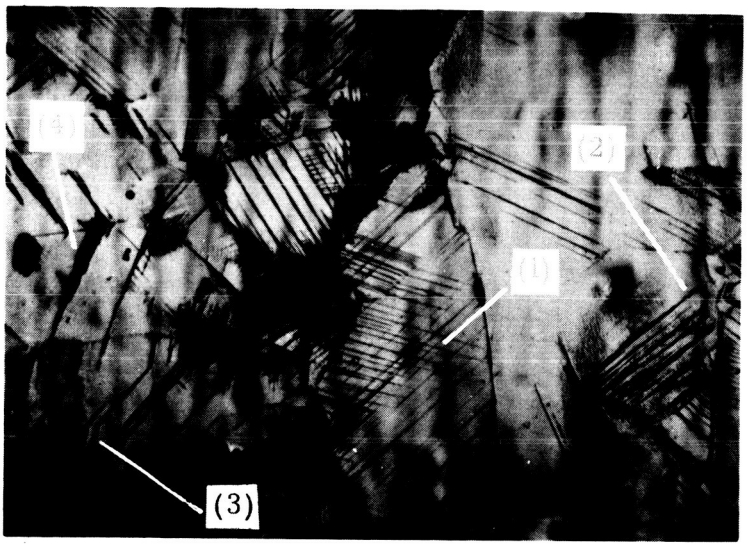

FIG. 37 ELECTROPOLISHED SURFACE OF RE-ANNEALED SPECIMEN. SECTION OF MAIN CRACK IS PERPENDICULAR TO THE STRESS AXIS. SLIP-ZONE MICROCRACKS AND CRYSTALLITE FORMATION. (A-6R, $\pm$ 12.0 ksi, x 100).

1. CROSS SLIP
2. DEFORMATION BANDS
3. QUASI-CLEAVAGE FRACTURE
4. LINK UP OF CROSS SLIP

FIG. 38 DIFFERENT SECTION OF CRACK SHOWN IN FIG. 37. KINK BAND FORMATION IN CENTER OF PICTURE. CONCENTRATED SLIP. (x 200).

1. GRAIN BOUNDARY
2. KINK BANDS
3. DEFORMATION BANDS

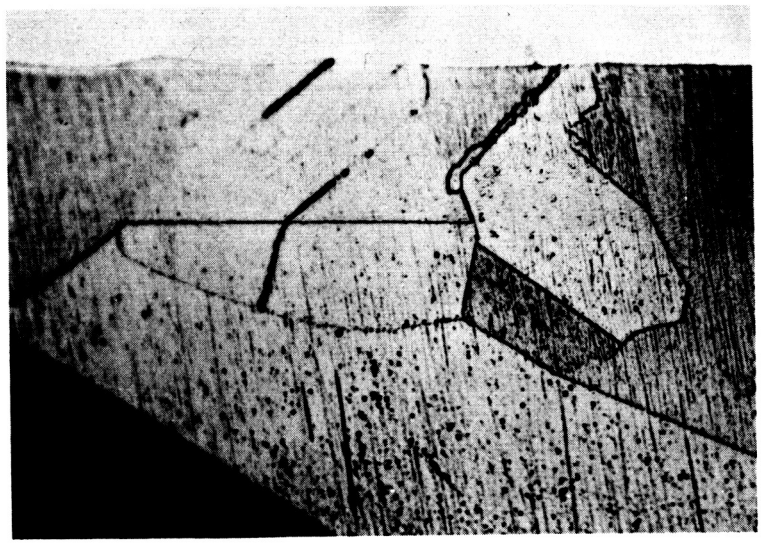

FIG. 39 SLIP-ZONE MICROCRACKS OF RE-ANNEALED ELECTROPOLISHED SPECIMEN SURFACE. (A-6R, $\pm$ 12 ksi, taper magn. x 3.7, optical magn. x 500).

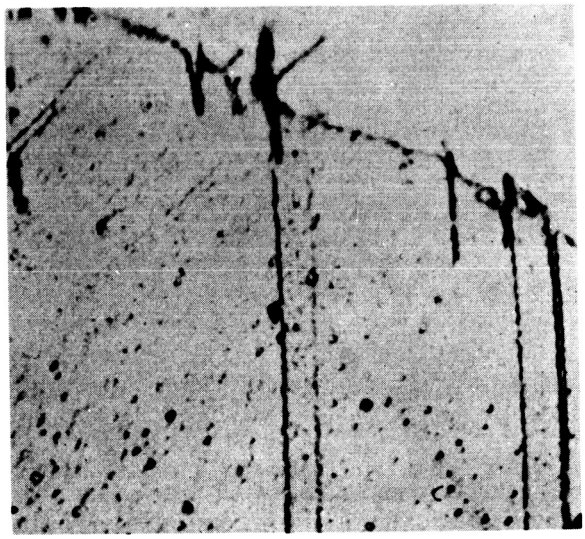

FIG. 40 NOTCH-PEAK EFFECT. (B-1R, $\pm$ 16.5 ksi, taper magn. x 3.7, optical magn. x 1000)

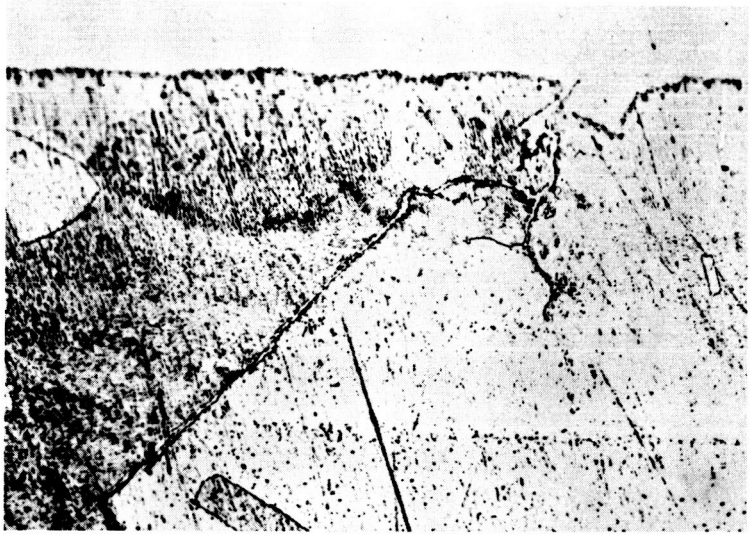

FIG. 41 GRAIN BOUNDARY MICROCRACK OF SPECIMEN SHOWN IN FIG. 40.

FIG. 42 LONGITUDINAL SECTION THROUGH CRACK. CRACK IN COMPRESSION HALF CYCLE OF STRESS AMPLITUDE. NOTE SECONDARY CRACK AT 45° TO MAIN CRACK. THE STRESS AXIS IS VERTICAL. (A-73 ± 14 ksi, 8.179 $(10)^5$ cycles, x 500).

1. FRETTING OF SURFACE

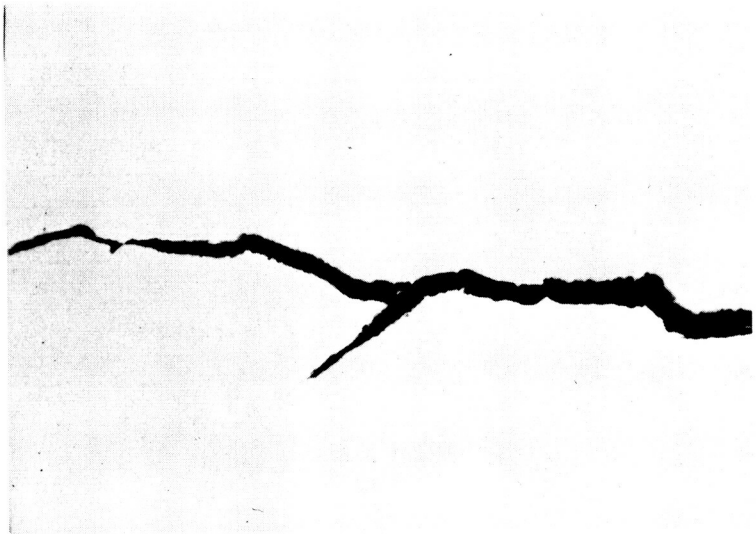

FIG. 43 UNETCHED SECTION OF SPECIMEN SHOWN IN FIG. 39 NOTE JUXTAPOSED DEPRESSIONS. (x 500).

FIG. 44 CRACK TIP PROFILE OF SPECIMEN SHOWN IN FIG. 39 ASYMMETRICAL TIP. (x 1000).

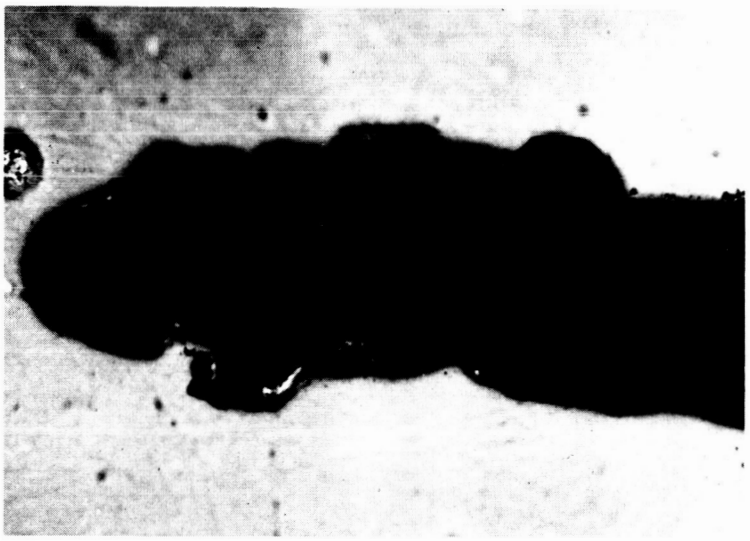

FIG. 45 CRACK TIP PROFILE OF SPECIMEN SHOWING FEATURES OF CRACK IN TENSION HALF CYCLE. (E-6, $\pm$ 10.0 ksi, 1.042 $(10)^7$ cycles, x 1000).

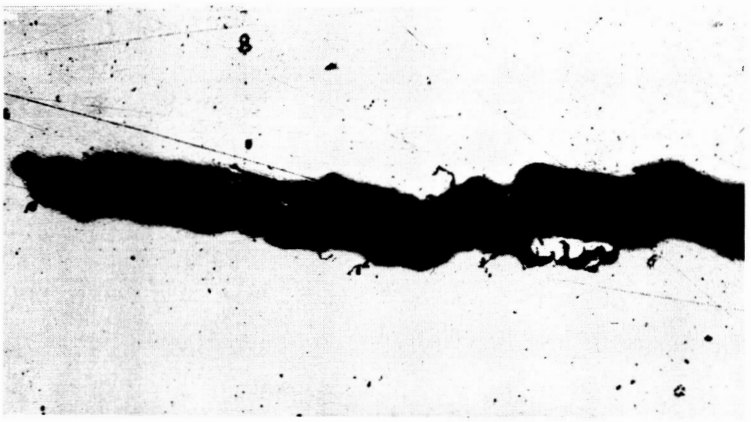

FIG. 46 CRACK TIP PROFILE OF SPECIMEN SHOWN IN FIG. 45. AFTER RE-POLISHING. (x 200).